Textural and spatial relationship between platinum-group elements and alteration assemblages in the Afton porphyry system, Kamloops, British Columbia

By Mark J. Garagan

A Thesis Submitted in Partial Fulfillment of the Requirements for the Degree of

Bachelor of Science (Honours)

(Geological Science)

Saint Mary's University, Halifax, Nova Scotia

April, 2014

Approved: Dr. Jacob

Hanley Associat

wProfessor

Table of Contents

Abstract

The Afton Cu-Au porphyry system is located near of Kamloops, B.C, Canada, and contains significant platinum-group element (PGE) enrichment. The alteration assemblages at Afton are consistent with a typical porphyry systems (phyllic, propylitic, potassic and argillic), with phyllic and propylitic being the most wide-spread and pervasive. Samples demonstrating elevated grades of Pd and Au show phyllic alteration is characterized by phengitic and paragonitic end-member dioctahedral micas (identified through NIR-IR spectroscopy and petrography). Two distinct mineralizing fluids are proposed, as phengitic micas require fluid-mobile Mg, whereas paragonitic micas will only stabilize in Mg-poor/alkali-rich fluids. However, both minerals require a fluid with a high pH. The samples demonstrate propyllitic alteration, characterized by Mg-chlorite, FeMg-chlorite, epidote and actinolite. Relative Au enrichment can show a positive correlation with Mg-chlorite. Mg-chlorite, similar to phengitic mica, requires a high pH and high Mg fluid to stabilize. Using SEM-MLA, Pd was found to be hosted within temagamite, and mertieite-II, most commonly in textural association with phengitic micas, and Mg-chlorite. 3D modeling (using Leapfrog and assay data) revealed a deposit-scale negative spatial correlation between Pd and primary Cu and Au, but a secondary, structurally-controlled relationship between Pd and Au. Preliminary IR fluid inclusion and LA-ICPMS studies revealed that primary fluid inclusions hosted with hematite are coeval with Pd deposition since Pd was found in trace amounts as a dissolved species in hematite at concentrations in the 100-200 ppb range. The results of the study demonstrate that Pd deposition occurred in response to secondary hydrothermal events involving oxidizing, high pH, Mg- or alkali-rich, and chloride-rich fluids (based on mineral chemistry) operating at conditions of ~400-500^{o}C and above 0.5 kbar (based on phengite-biotite stability in absence of talc). Degassing of high Mg basaltic subvolcanics, now spatially associated with the porphyry stock, may have been the source of these Pd-rich fluids.

Acknowledgments

I would like to thank Dr. Steve Piercey and Jean-Luc Pilot (PhD candidate for them allowing the use of the TSG-terraspec software, along with their knowledge about the software. Additionally I would like to thank Dr. Dan Laytton-Mathews and Agatha Dobosz from Queen's University for allowing the use of the SEM-MLA, along with their knowledge with regards to the equipment and assistance in mineral identification. I would again like to thank Dr. Jacob Hanley for guiding me through this project and his expert knowledge on palladium mineralization. I would like to thank Fergus Tweedale (M.Sc) and Saint Mary's University for his knowledge and assistance with SEM work. Finally I would like to thank New Gold Ltd. for project funding and providing the necessary samples used in this study.

1.0 Introduction

Platinum-group elements (PGE) have been noted to occur in alkalic porphyry systems around the world. Examples of such deposits are: Mt Milligan, Galore Creek, Skouries, and Elatsite (LeFort et. al, 2011; Hatch, 2006; Kiousis, et al. 2005; Augé et al., 2005). These subduction-related deposits (Economou-Eliopoulos, 2005) are found in British Columbia, Eastern Europe, and the South Pacific. It has been suggested that the Pd enrichment in these deposits is related to alkaline arc magmatism, derived from a PGE-enriched mantle source (Thompson et al., 2001), however, there is much debate regarding the processes responsible for PGE deposition and mineralization. The primary focus of this study will be to characterize the processes responsible for the deposition of PGE at the Afton Cu-Au porphyry system in Kamloops B.C. This will be accomplished by examining the relationship between PGE distribution and mineralogy and alteration styles. In addition, with the use of these relationships, the study aims to develop exploration criteria for PGE bearing porphyry systems globally.

2.0 Geological setting and background

2.1 Platinum group element solubility

The stable oxidation state for Pd in an aqueous solution is $Pd^{2+,}$ and in such a state it tends to form complexes with ligands such as HS^- and Cl^- (Economou-Eliopoulos, 2005). Palladium is soluble over a range of hydrothermal conditions. In hot and highly oxidized solutions Pd tends form chloride complexes; whereas in hot and reduced solutions, Pd is more like to form bisulfide complexes (M. Economou-Eliopoulos, 2005, Hanley, 2005, Wood, 2002). Around 300ºC and at a pH <6, Pd-chloride complexes can only form at strongly oxidizing conditions. However, at a pH <3 at 300^0C, strongly oxidizing conditions

are no longer required and these chloride complexes can form under relatively reducing conditions at low pH and high fo_2 (Wood, 2002), therefor as a rule, the concentration of Pd-chloride complexes will be maximized and thus the potential for Pd to be precipitated as a result of a changing conditions from strongly oxidising and acidic conditions to more reducing and neutral conditions is significant (Wood, 2002). In a solution enriched in other metals that also favor chloride ligand complexes (Cu^{+}, $Fe^{2+,}$ and Mg^{2+}), the concentration of Pd in solution will consequently decrease due to the ligand cation competition for chloride (Wood, 2002, Economou-Eliopoulos, 2005, Hanley, 2005). As Pd, Au and Cu can be transported by the same ligands, it has been suggested that these transported deposition mechanisms may result in a strong genetic and spatial association between the mineral phases hosting these elements (Economou-Eliopoulos, 2005). However at the Afton porphyry deposit, PGE enrichments are completely decoupled from Cu and to a lesser extent Au in the ores.

2.2 Platinum group elements in porphyry systems

Palladium enriched porphyry systems are generally associated with alkaline rocks in which the silica content is less than 60% (Economou-Eliopoulos, 2005). Parental magmas associated with these systems typically contain a high dissolved volatile content and are moderately fractionated (Eliopoulos et al., 1995). Copper mineralization is represented by bornite and chalcopyrite, with associated pyrite and magnetite. Parental magmas responsible for alkaline porphyry systems are thought to be very hydrous and oxidized, which gives rise to their ability to form hydrothermal systems that are ideal for transporting metals like Cu and Pd by chloride complexation (Economou-Eliopoulos, 2005). These parental magmas also contain abundant SO_2 and CO_2, which strongly impact fluid

evolution because these dissolved gases exsolve from aqueous volatiles fluid during cooling, leading to a development of extensive brecciation zones (Economou-Eliopoulos, 2005). Palladium mineral distribution in other alkaline systems commonly show a positive correlation with Cu and early potassic alteration, leading to the conclusion that Pd and Cu were deposited during early stage alteration (during the main porphyry stage event) in the central parts of the porphyry, along its flanks, and in the cupola zone. However, as mentioned before, the same general association is not seen at all portions of the Afton deposit.

2.3 Regional geology

Within the Afton region there are rocks of Cenozoic, Mesozoic, and Paleozoic ages. The Upper Triassic units are of the most economic significance at the Afton deposit. The significant formations are the Nicola Volcanic group (205-220 Ma), ranging in composition from low alkaline to shoshonitic (Mortimer, 1987), and the Iron Mask Batholith (Dolbear, 2004), which is a porphyry intrusion, containing compositions ranging from syenitic to dioritic. Compositionally, the Iron Mask Batholith is alkaline to sub-alkaline. The Iron Mask Batholith is eighteen kilometres in length and strikes to the northwest (Dolbear, 2004). These rocks have been interpreted to represents an island arc volcanic zone, with the Iron Mask Batholith representing the shallow plutonic core of this system (Dolbear, 2004). The mineralization zone at the Afton deposit is located in the northwest extremity of the Iron Mask Batholith, in an early Jurassic unit called the Cherry Creek Unit (204 Ma) (Dolbear, 2004, Mihalynuk, et al. 2006).

2.4 Local geology

The Cherry Creek Unit, a highly altered syenitic micro-diorite (Dolbear 2004), is the main ore-hosting unit in the mine. Small high Mg basaltic dikes and sills are found sub parallel to the Iron Mask batholith within the syenite units, and are mapped historically as picrites (Fig. 1). Parallel to the basalt bodies in the southern portion of the deposit, rare latite dykes have also been noted, with a thickness up to 20 meters (Dolbear 2004). The main ore zone appears to be fault-controlled and has both Cu- and Au hosting phases disseminated throughout. The fault zone is 80 to 130 meters wide, and is steeply-dipping to the southeast, and striking to the north east. The main zone is tabular in shape, southwest-plunging, and parallel (in conjunction with) the previously mentioned fault (Dolbear, 2004). The upper 300-400 meters of the deposit consists of a supergene zone, with the main Cu ore minerals being native Cu, chalcocite and cuprite. In addition to the Au- and Pd-bearing minerals, the lower hypogene zone consists of mainly bornite and chalcopyrite, with minor native Cu. Grade ratios do not change from the supergene to the hypogene zones (Dolbear, 2004). The northwestern portion of the Afton main zone is said to be in contact with a "pebble-breccia conglomerate-like unit" or a pebble dike on the hanging wall.

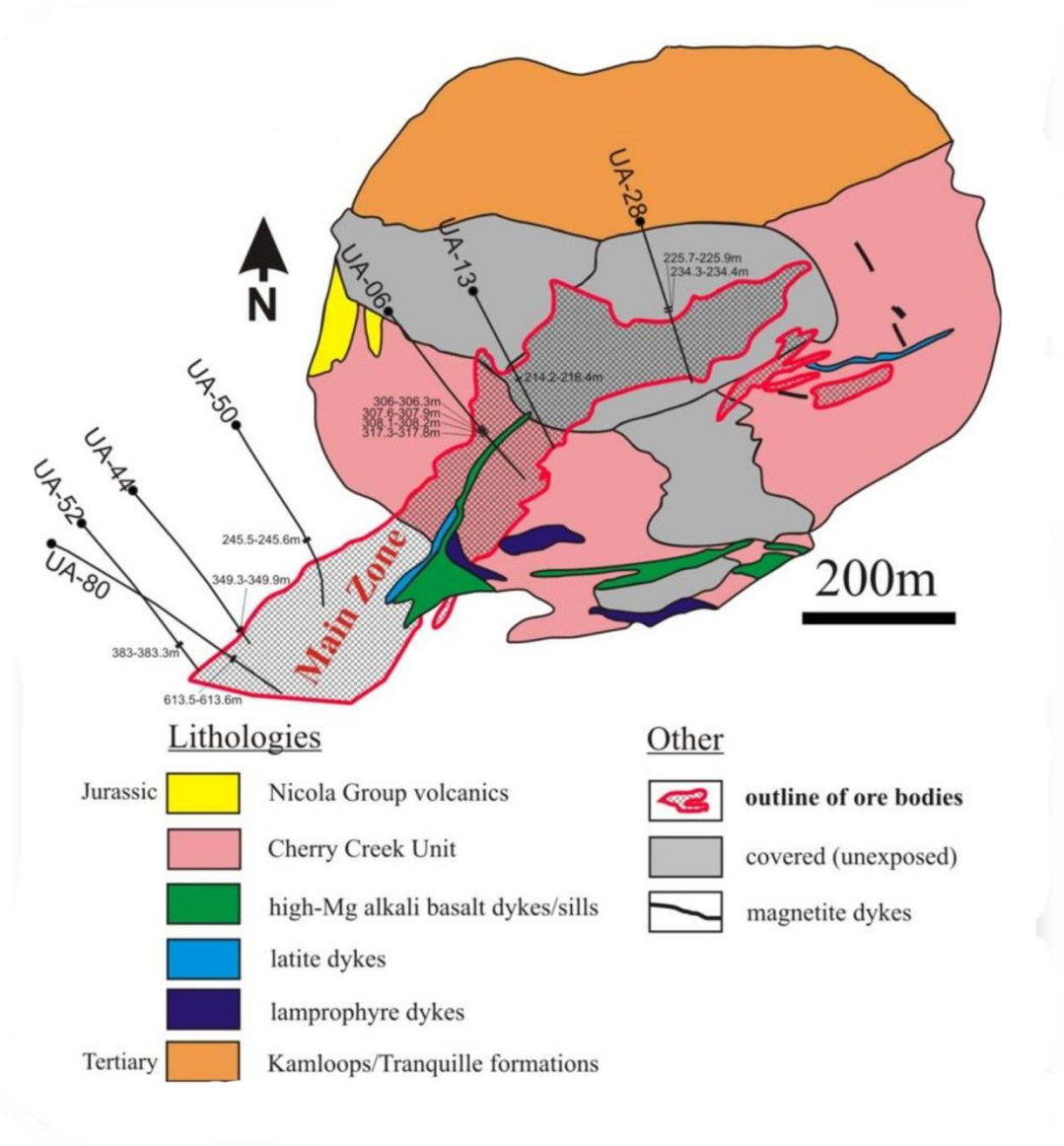

Figure 1. Plane view geological map of Afton Pit and main zone. Labeled are the drill holes used for this study.

3.0 Methods

3.1 Infrared and near-infrared spectroscopy

Infrared spectroscopy was conducted at Memorial University in Saint John's, Newfoundland. A Terraspec 4 high resolution mineral spectrometer was used in conjunction with Spectral Geologist (TSG 7) software to determine the main alteration mineral phases present in the samples. Forty-three samples from eight different drill holes where selected for IR spectroscopy. The samples were selected because they displayed a variety of alteration assemblages in hand sample, and variations in precious metal (PGE, Au) grades. Both diamond drill core sample intervals and powdered samples were used during IR spectrographic studies. A ceramic plate was used for a white balance standard test. This test is important to assure the instrument is calibrated properly. Pure samples of both talc and pyrophyllite were used as reference standards (Memorial University) to confirm the accuracy of the TSG software. The sofrware would identify both talc and pyrophyllite with a known composition accurately each time the standards were analyzed. In addition to this, as each sample was analyzed 3 times, each time the analysis yielded the same dominant minerals and associated spectrum. Each sample was analysed by placing it on top of the stationary spectrographic device. At the top of this device, light passes through a 4 cm-diameter circular opening which represented the area being analyzed. Samples were held over the light. Spectra would be collected and created by the Terraspec software over an interval of 15 seconds. The software would repeat the analysis every fifteen seconds on the same sample position. When the created spectra became stable in shape and intensity, the TSG would collect the next spectra. The sample would then be moved as to collect a new spectra on a different position of the same sample. Each sample was analyzed 3 times

where areas appeared mineralogical representative of the slab and homogeneous by visual inspections. Veins and sulfide rich zones were avoided in attempt to produce a data set that best represented the alteration mineral assemblage in the host lithology. Both the white balance and the reference mineral tests were conducted prior to the analysis of each sample. If the spectra produced for the reference minerals were not correct, the instrument was recalibrated.

3.2 3D modeling using Leapfrog software

Drill hole sample locations and subsequent Pd, Au and Cu assays, in ppm and wt% Cu, respectively, were plotted using Leapfrog geo 1.4 3D software. Drill collars and elevations were plotted. Polygon plots were constrained to 50 ft boundary limits in the x,y and z directions. Any smaller than the set 50 foot extrapolation limit and the polygons would not connect to one another and instead would only form isolated polygones around the specific point. Any larger than the set 50 foot extrapolation limit and the area of the polygons were too large to be considered reasonable for the limited amount of data available. For each element four zones (represented by different colours) were characterized to represent high, high medium, low medium and low grades. The designated zones for elements were all different, and based upon the spread of concentration grade for each element. For Au, the respective zones were: greater than 1.4, 1.4-3.0, 0.6-1.4 and <0.6 ppm. For Cu these values were: >1.8, 1.0-1.8, 0.4-1.0, and <0.4 wt% Cu. For Pd these values were: >0.93, 0.66-0.93, 0.57-0.66, and <0.57 ppm. Cross sections (Fig. 12) and plan sections (Fig 14) were created throughout the deposit. Three plane sections were created at different elevations, one near the surface, the second around 121.9 m (400 ft) in depth and the third around 182.88 m

(600 ft) in depth. Cross sections were created in intervals along the north-south plane, sub-perpendicular to the main fault. The cross sections were created on the far eastern and western ends of the deposit and, along its center.

3.3 Scanning Electron Microscope-Mineral Liberation Analyser (SEM-MLA)

Three polished thin sections were prepared by Vancouver Petrographics for scanning electron microscope-mineral liberation analysis (SEM-MLA). SEM-MLA was conducted at Queen's University in Kingston, Ontario. Each sample was scanned twice. First, the entire sample was scanned for approximately 3 hours. This first scan was used to identify the main mineral phases in the samples. Second, the sample was scanned for 5 hours, to determine as many precious mineral phases as possible. The second scan lasted for approximately 5 hours per sample. This scan was designed to only scan areas in which there were trace minerals of high density; scanning was done at a pixel size was equivalent of 0.1 micron. A smaller scan zone was used for the second scan to attempt to identify as many of the trace PGE and accessory phases as possible, in a reasonable time frame. Using the MLA software, similar spectral data were categorised into groups. These spectral data were compared to a database of minerals created by the Geology department at Queen's University to determine which spectra corresponded to which minerals. Minerals in which there were no species present in the Queen's database were classified by examination of the chemical composition of the analyzed species using SEM software to determine how much of each element was present in that specific mineral. These minerals were than given a name depending on their chemical composition, with comparison to previous work (Lefort et al., 2011).

3.4 LA-CPIMS and bulk rock geochemistry

Trace elements in hematite were quantified by laser ablation ICP-MS at ETH Zurich, Switzerland. Ablation was performed with a fluence of 15 Jcm^{-2} using a prototype system similar to the available from GEOLAS (now Coherent Inc.) with a homogenized 193 nm ArF Excimer laser (Günther and Heinrich, 1999). Aerosols were generated using a pulsed beam at 10 Hz and 80-90 mJ output energy generated aerosols. Ablation pit diameters were set to 50 microns. An Ar-He gas mixture (He 1.15 L/min; Ar 0.8 L/min) carried sample aerosols into an ELAN 6100 quadrupole ICPMS using similar conditions as Pettke et al. (2004). A representative signal is shown in Figure displaying the typical intensities for elements. Oxide production rates were maintained below 0.3 percent. Mass spectrometer dwell time was set to 10 ms for all masses measured and quantified. Quantification of trace element concentrations was performed using the software SILLS (Guillong et al., 2008). The standard reference glass 610 from NIST (National Institute of Standards and Technology) was used in the calibration of analyte sensitivities and the Fe content of ideal hematite was used for internal standardization.

Bulk rock samples were analyzed for trace elements including the PGE and Au at the Ontario Geoscience Laboratories (Sudbury, Ontario). Most trace elements were analyzed by solution ICP-MS after a closed-vessel multi-acid digestion, with the exception of the PGE and Au that were determined using Ni fire assay followed by telluride precipitation and ICP-MS finish. Overrange values for the base metals (e.g., Cu) were determined using AAS.

4.0 Results

4.1 Alteration

There are six different alteration assemblages recognizable in hand sample and thin section from the ore zone and its associated host units at the Afton mine. These assemblages are: phyllic, potassic, propylitic, argillic, iron oxide-rich supergene, and silicified.

The iron oxide zone represents the supergene enrichment zone in the upper portion of the ore body. This zone is characterized by chalcocite, bornite and native Cu. Copper and Au grades within this zone are similar to those within the hypogene zone (Dolbear 2004). Silicification (silica flooding) can be identified by annealed silica around quartz veins. The silicified alteration is present in the majority of samples, and is not related to of high Pd or Au grades.

Phyllic alteration, the most common alteration style in ore samples analyzed, identified and is characterized by the presence of sericite. Phyllic alteration within the sample suite is strictly pervasive (Fig. 2A&2B). NIR-IR Spectroscopy classified the majority of samples with pervasive phyllitic alteration as containing paragonite [$NaAl_2(AlSi_3O_{10})(OH)_2$], illite [$K_{0.65}Al_2(Al_{0.65}Si_{3.35}O_{10})(OH)_2$] or Phengite [$K(Al,Mg)_2(OH)_2(Si,Al)_4O_{10}$]. Due to the prevalence of phyllic alteration and its association with a range of grades, it is not indicative of variations in Au or of Pd grade (Fig. 2C-2G).

There are two forms of potassic alteration, both characterized by the presence of biotite. One style of potassic alteration is fracture-controlled and, selectively pervasive (Fig. 2C&2D). This hydrothermal biotite commonly displays reaction textures (replacement) by fracture-controlled chlorite. Samples with pervasive potassic alteration tend to display high grades of both Au and Pd, up to 2.7 ppm and 2.9 ppm respectively. The second style of

potassic alteration is predominantly pervasive, characterized by biotite and K-feldspar. This style shows significantly lower Au and Pd grades and is commonly overprinted by primary phyllic and propylitic alteration styles, thus representing an earlier event, and not directly related to the Au and Pd mineralizing event.

Propylitic alteration, characterized by chlorite, epidote and actinolite, most commonly occurs in the outer-most portion of porphyry deposits at depth (Allen et al. 1996). Very common in the sample suite, propylitic alteration is almost exclusively selectively pervasive and fractured controlled (Fig. 2E, 2F). In rare cases, chlorite has replaced the primary potassic alteration pervasively. When the primary style of alteration is propylitic, there tends to be high Au grades and respectively lower Pd grades, around 2.6 ppm Au and 0.8 ppm Pd. These Pd grades are still however significant. Infrared spectroscopy revealed two major types of chlorite: Mg-chlorite (clinochlore) and Fe-Mg-chlorite (chamosite). When Mg-chlorite was the primary chlorite phase, Au grades tended to be enriched relative to the rest of the samples. However when Fe-Mg chlorite was present, Au grades were relatively depleted. Pd did not show any significant correlation to the type of chlorite present in the sample, varying from low grade to high grade in both Fe-Mg chlorite and Mg-chlorite dominated samples.

Argillic alteration tends to be texturally destructive of igneous fabric, and structurally controlled (Allen, et al. 1996), of which both can be noted at Afton (Fig 2G, 2H). Argillic alteration is characterized by clays, usually kaolinite. Similar to the hydrothermal potassic alteration, Au and Pd grades seem to be enriched in samples containing argillic alteration.

4.2 Infrared and near infrared spectroscopy

The major alteration mineral end members identified using IR and NIR spectroscopy were Mg-chlorite, FeMg-chlorite, muscovite, illite, phengite, paragonite, epidote and kaolinite. Of these minerals, the most important with respect to Pd and Au grades were Mg-chlorite, paragonite, and phengite. The spectroscopic analysis also identified mixtures of several minerals based on a Al absorption band displacement feature, these minerals are phengitic and paragonitic end member dioctahedral mica. Increase in Au grade (above 1.0 ppm) showed a positive correlation with Mg-chlorite. Increases in Pd grade (above 0.7 ppm) tended to show a positive correlation with phengite (Table 1). Pd in some cases showed an increase when Au had a high concentration. Palladium grade and Au grade show a positive correlation when both Mg-chlorite and paragonic end-member or phengitic end-member dioctahedral micas are present. Although they do show a positive correlation under these circumstances, there are some instances in which the grade does not correlate with this mineral assemblage. Phengite and paragonitic-illite/illite were differentiated based on an Al-OH absorption feature around 2200 um and 2220 um, whereas chlorites were differentiated by their Mg:Fe ratio (Fig. 3-6). The position of the aluminum feature and the TSG logs were summarized with Au and Pd grades to show how alteration mineralogy relates to grade (Table 1).

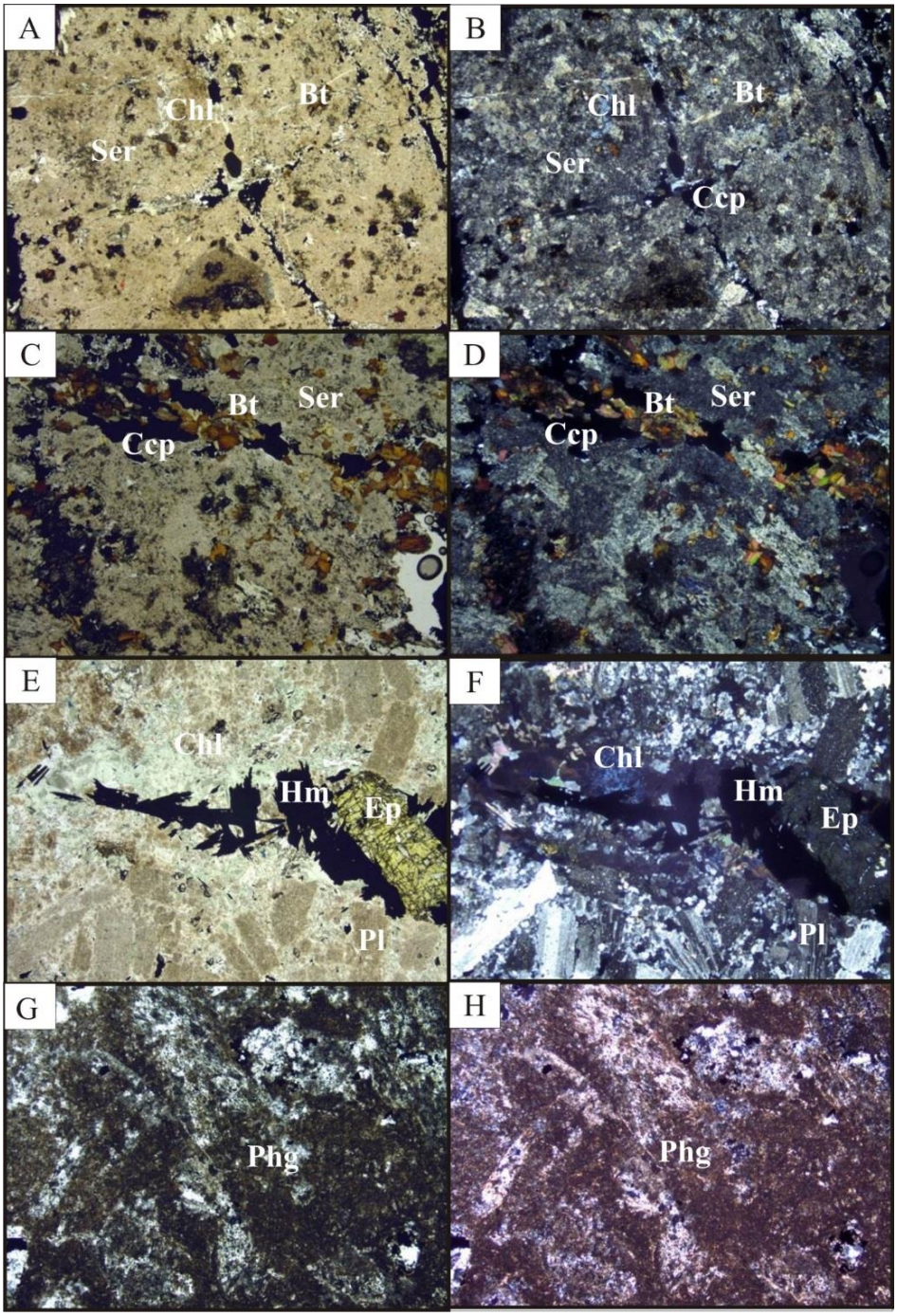

Figure 2. Transmitted light microscope pictures of all alterations styles: (A&B) plane polarized (PPL) and crossed polarized light (XPL) photos of pervasive phyllic alteration, along with trace amounts of fracture controlled propylitic alteration. PPL (C) and XPL (D) photos of selectively pervasive fracture controlled potassic alteration, characterized by biotite. Pervasive phyllic alteration is also present. PPL (E) and XPL (F) photos of selectively pervasive propylitic alteration, characterized by chloride and epidote. PPL (G) and XPL (H) photos of destructively pervasive argillic alteration.

Table 1. Summary of NIR-IR characteristics and grade characteristics

Drill hole	From (ft)	To (ft)	Absorption Feature(um)	Al content	White Mica	Chlorite	Other	Pd (ppm)	Au/Pd	Cu (wt%)	Au (ppm)	Pd/Cu
UA 28	225.6	225.	2.206-2.208	High Al	paragonitic illite	Mg		0.36	5.71	1.856	2.054	0.193
	226.5	226.	2.204-2.207	High Al	muscovite	FeMg		barren				
	230.43	230.	2.209-2.209	Low Al	phengiticillite	Mg		0.294	4.43	1.372	1.301	0.214
	232.13	232.	2.208-2.210	Low Al	phengite		kaolinite	barren				
	234.8	234.	2.203-2.204	High Al	phengiticillite		kaolinite	1.001	2.76	1.7242	2.763	0.580
UA 06	300.7	300.	2.207-2.210	Low Al	phengiticillite	FeMg		barren				
	306.04	306.				Mg		1.293	8.71	5.9369	11.257	0.217
	307.59	307.				Mg		0.818	27.14	6.8073	22.2	0.120
	308.1	308.				Mg		0.477	20.63	5.6428	9.841	0.084
	317.32	317.	2.210-2.213	Low Al		FeMg		0.154	6.47	4.8948	0.996	0.03
	321.2	321.				FeMg		1.36	2.76	7.4044	3.76	0.183
UA 44	343.45	345.	2.206-2.207	High Al	paragonitic illite	FeMg	epidote	0.436	0.08	0.0946	0.0336	4.608
	344.95	345.	2.209-2.210	Low Al		Mg	epidote	3.15	0.07		0.23	
	345.7	345.				FeMg	ankerite	0.102	0.40	0.1807	0.0412	0.564
	348.9	349.	2.205-2.207	High Al	paragonitic illite	Mg	epidote	1.122	2.40	3.1184	2.688	0.3598
	349.31	349.	2.203-2.207	High Al	paragonitic illite	Mg		2.941	0.93	3.4445	2.742	0.853
	349.51	349.	2.205-2.207	High Al	paragonitic illite	Mg	phlogopite	barren				
UA 50	227.2	227.				FeMg		barren				
	228.13	228.	2.204-2.207	High Al		FeMg	dolomite	0.5	0.32	3.9952	0.16	0.125
	228.9	229	2.204	High Al			kaolinite	0.5	0.32	3.9952	0.16	0.12
	241.22	241.				FeMg		2.627	0.41	1.4612	1.073	1.797
	245.7	245.	2.208-2.210	Low Al	phengitic-illite	FeMg		0.439	9.27	2.6076	4.068	0.168
UA 52	382.35	382.	2.211	Low Al		FeMg	ankerite	barren				
	383	383.	2.209-2.210	High Al		FeMg		0.823	3.15	1.5217	2.593	0.54
UA 80	612.87	624.			phengite	Mg		barren				
	613.2	613.			phengite	FeMg		barren				
	613.5	613.	2.214-2.219	Low Al	phengite	FeMg		0.818	2.62	2.0438	2.141	0.40
	617.65	617.	2.207-2.209	High Al	paragonitic illite	Mg		0.067	11.10	0.6966	0.744	0.096
	618.3	618.	2.205-2.209	High Al	paragonitic illite	Mg	phlogopite	0.06	14.40	0.8255	0.864	0.078
UA 100	820.12	820.	2.204-2.205	High Al	paragonitic illite			barren				
	822.75	822.	2.212-2.213	Low Al	phengiticillite	FeMg		0.709	0.46	0.576	0.327	1.230
	823.16	823.	2.212-2.213	Low Al	phengite	FeMg		barren				
	828.4	828.	2.213-2.215	Low Al	phengiticillite	FeMg	ankerite	barren				
	838.1	828.	2.204-2.206	High Al	muscovite			barren				

The white mica feature is related to position of depression relating to the Al content of dioctahedral micas. The lower the absorption feature value, the higher the aluminum content in the mineral.

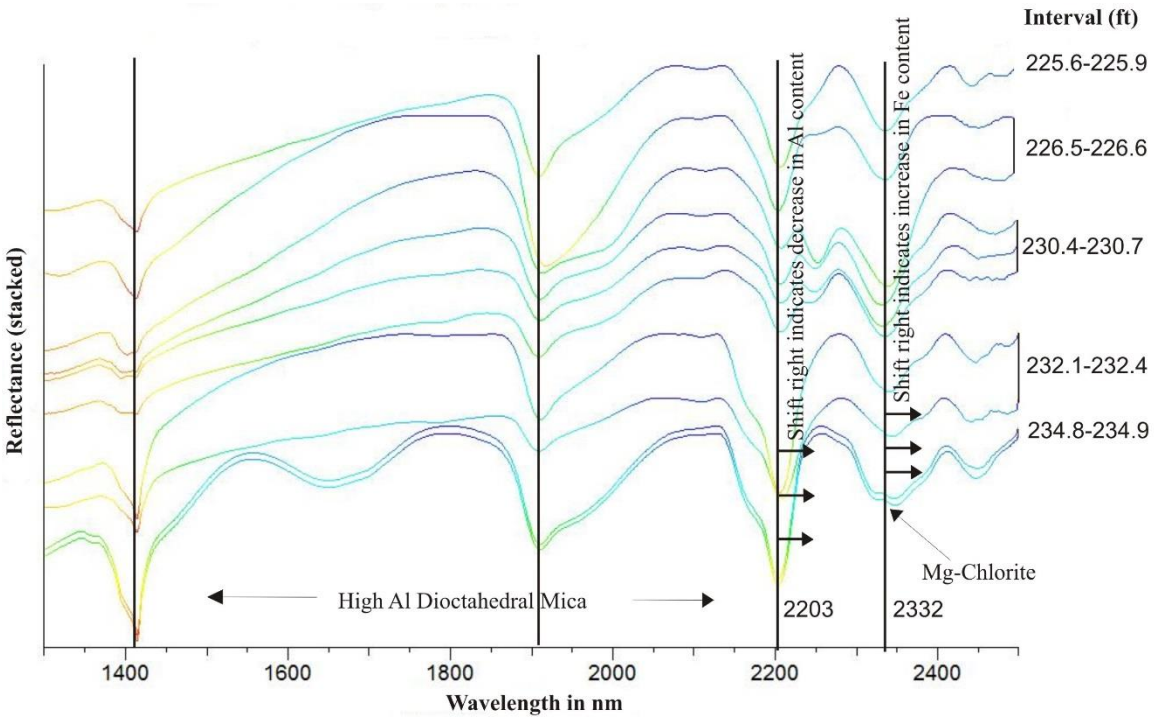

Figure 3. TSG created near infrared spectra for samples from hole UA28: The absorption feature at 2203um represents the Al-OH absorption feature, shifts in this band to the right represent a decrease in Al content of the dioctahedral mica. The absorption feature labeled 2332um represents Mg-rich chlorite, shifts in this band to the right represent an increase in Fe content of chlorite. Other depressions are related to quartz and kaolinite or are a result of the mixture of two minerals.

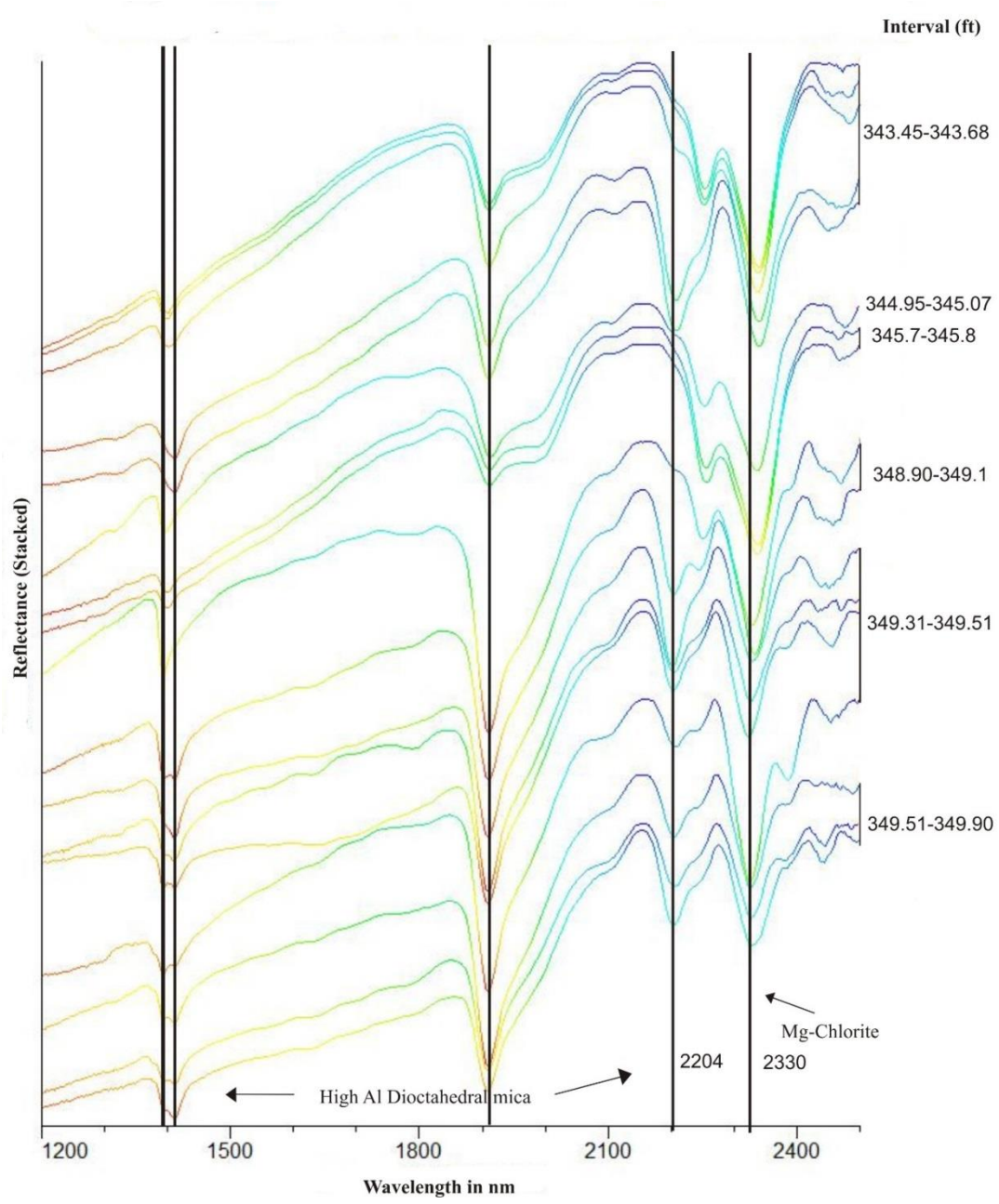

Figure 4. TSG created near infrared spectra for samples from hole UA44: The absorption feature at 2204um represents the Al-OH absorption feature. The absorption feature labeled 2330um represents Mg-rich chlorite. Refer to Table 1 for log of spectra.

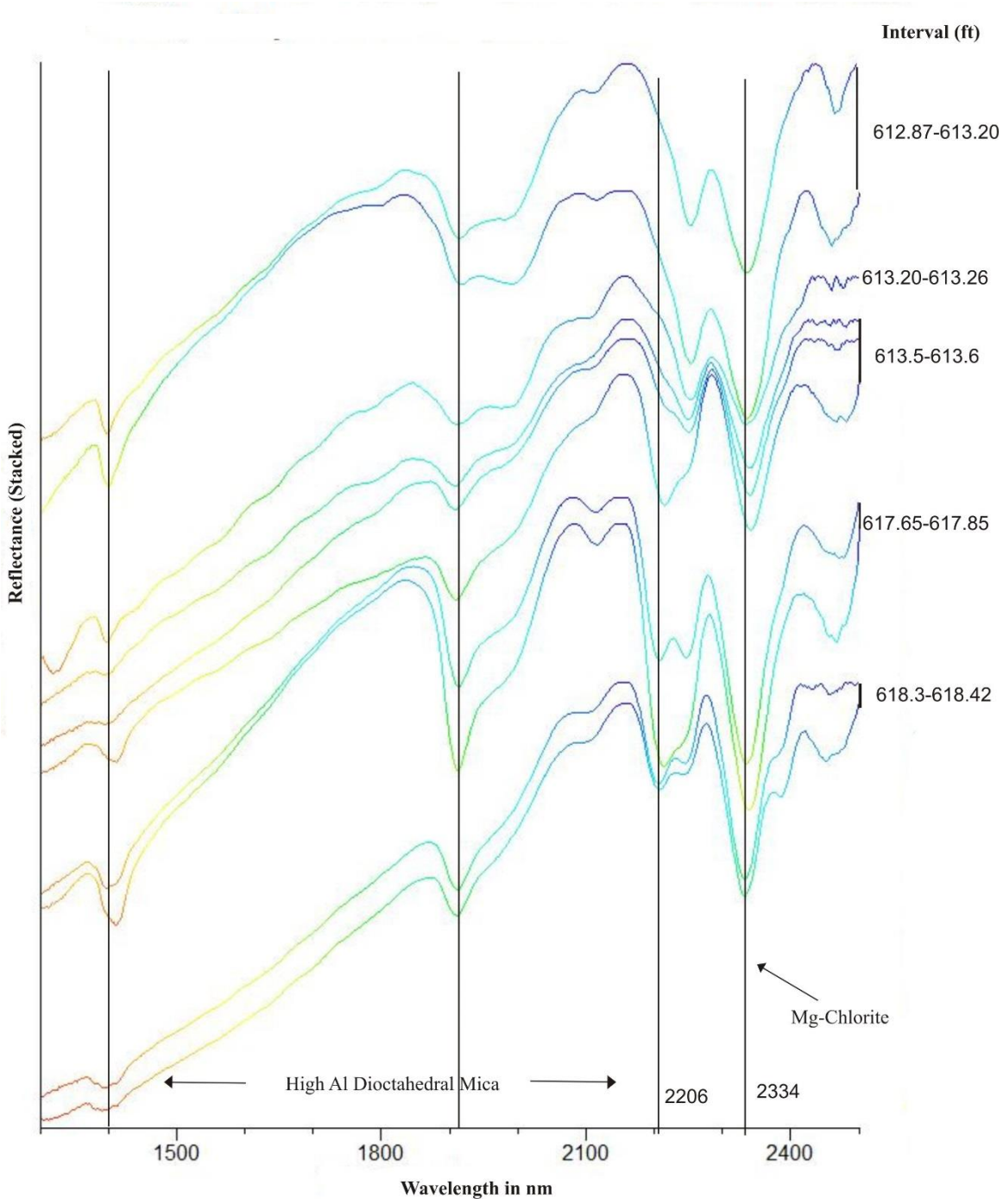

Figure 5. TSG created near infrared spectra for samples from hole UA80: The absorption feature at 2206um represents the Al-OH absorption feature. The absorption feature labeled 2334um represents Mg-rich chlorite. Refer to Table 1 for log of spectra.

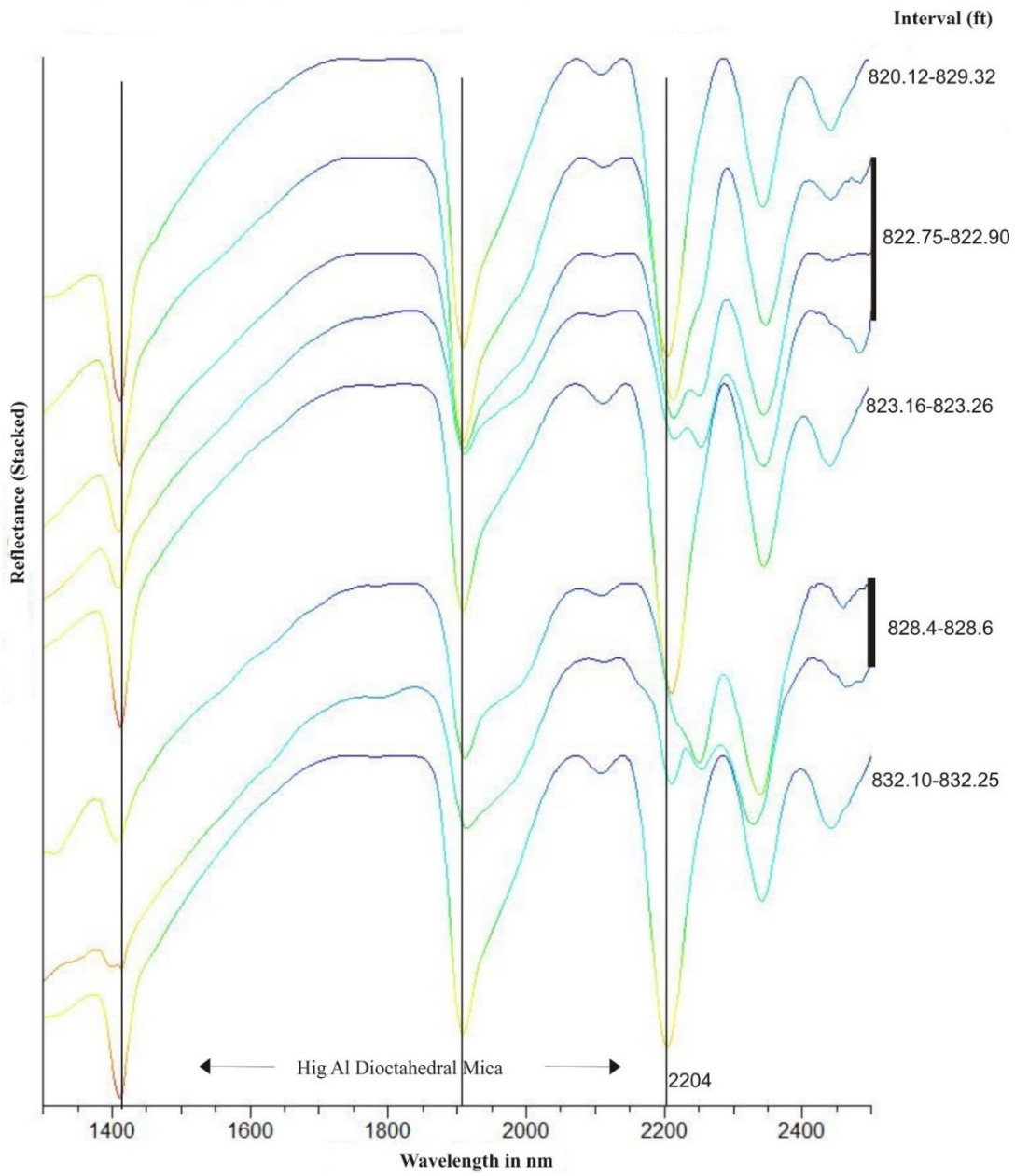

Figure 6. TSG created near infrared spectra for samples from hole UA100:

The absorption feature at 2204um represents the Al-OH absorption feature.

4.3 Scanning electron microscope-mineral liberation analyses

Comparison of the mineral assemblages were conducted through SEM-MLA, petrography and IR-spectroscopy studies. Using spectral data produced by the SEM-MLA software, the main Pd-bearing phases were identified along with their mineral host phase. The different phases hosting, and in association with, Pd-bearing minerals, along with their relative modal percentages were determined (Table 2). In the 3 samples analyzed using the SEM-MLA, the PGE phases were; temagamite (Pd_3HgTe_3), mertieite-II [$Pd_8(Sb,As)_3$] and sperrylite ($PtAs_2$). Gold was found in the form of electrum and, in rare cases, as an Au-Ag-Zn-Cu alloy. In addition to these, other minerals of interest were found, specifically Ta and Ag phases. The silver minerals were kurillite (Ag_8Te_3Se) and naumannite (Ag_2Se), and the Ta phase was tantite (Ta_2O_5). Two samples analyzed using the SEM-MLA displayed similar alteration styles and one displayed a very different style. All three samples displayed varying Au, Pd and Cu grades.

Sample UA50 241 (1.07 ppm Au, 2.63 ppm Pd) contained only temagamite as the discrete PGE carrier, the majority of which was hosted within, with decreasing abundance, apatite, quartz, chalcopyrite and ankerite/calcite (Table 2). This sampled showed the highest grade of the three sample suite, with a Pd grade of 2.62 ppm (Fig. 10). Although apatite is listed as the primary host, temagamite was found within fractures of apatite with quartz, chalcopyrite, and ankerite/calcite (Table 2). Temagamite is not strictly hosted within apatite, rather in quartz-carbonate veins and chalcopyrite. This is an example of one of the limitations of this program, in which to get around one must be diligent about what is produced from the MLA. In this case, apatite acts as the brittle host breccia for the

mineralization. As this sample is mainly brecciated apatite with quartz, carbonate, chalcopyrite and hematite, no alteration style has been assigned.

Sample UA 50 245.4 (4.07 ppm Au, 0.44 ppm Pd) had Pd hosted within temagamite and mertieite-II, Pt hosted within sperrylite, and Au hosted within electrum and an unknown Ag-Au-Cu-Zn alloy (Table 3). This sampled displayed the highest Au grade and lowest Pd grade within the sample suite at 4.00ppm Au and 0.439 ppm Pd. Temagamite was hosted primarily within chalcopyrite, which very commonly was in contact with Mg-chlorite (Table 2). Mertieite-II was distributed evenly between both chalcopyrite and Mg-chlorite (Table 2). This sample displayed pervasive phyllic alteration with fracture controlled potassic and propylitic alteration. Within this sample both biotite and chlorite, and phengitic end member dioctahedral mica (low Al-dioctahedral mica) and plagioclase were found in conjunction with one another, commonly displaying reaction textures (Fig. 11).

Palladium in sample UA44 348 (2.69 ppm Au, 1.12 ppm Pd) is hosted within mertieite-II. Mertieite-II was hosted within dioctahedral micas (phengitic end-member to illite end-member) (Table 2), both of which make up the matrix and are a part of the pervasive phyllic alteration (Table 2). UA44 displays a strong pervasive phyllic alteration with fracture controlled potassic alteration. Phyllic alteration in this sample is subsequently stronger than that in UA50 245. Along with phyllic alteration being less pervasive in UA50 245, there is more illite compared to that of UA44, where there is respectively more phengitic end member dioctahedral mica. This supports the conclusion made via IR-Spectroscopy that sericitic-illite has a stronger correlation with Pd than illite.

In summary, the majority of Pd found through MLA studies is hosted within temagamite, with a less abundant amount within mertieite-II. The main binary host phases, which represent a situation when the entirety of the PGM is hosted within one mineral phase, was quartz and hematite. The major ternary host phases are chalcopyrite, apatite, Mg-chlorite and phengite. Ternary phase % represents situations in which the PGM is in contact with multiple mineral phases, and these minerals phases are assigned a percent based on the relative surface area they are in contact with the PGM (Table 2). Both Pd minerals appear to be hosted within secondary quartz carbonate veins or are immediately adjacent to such structures. In some instances, chalcopyrite is the host of Pd-bearing minerals (Table 2), where in others chalcopyrite is brecciated by the Pd-bearing quartz/carbonate phases (Fig. 10). Biotite with a higher than normal concentration of chlorine are commonly found adjacent to these Pd bearing features, along with phengite.

4.4 3D modelling using Leapfrog software

Three cross sections, three plane sections and three long were created using Leapfrog from for each element of interest, Au, Pd and Cu. The highest Au zone, characterized by overall grade, in g/t, (>3.0 ppm), appears to be concentrated in the center of the deposit at a depth of about 400ft (Fig. 12D, 12G). This high grade zone shows a WSW-dipping trend, which also becomes larger in area with depth (Fig. 12A). The maximum depth of this zone, extends to a depth of about 1000 meters in the WSW area of the deposit. The planview sections show very similar results as the cross sections (Fig. 14A, 14D, 14G). The long sections (N-facing) depict the strike of the Au-rich zone very nicely (Fig. 13A, 13D, 13G).

The Cu high grade zone (>1.8 ppm) is represented by a lens-shaped zone with its center at about 300 feet in depth (Fig. 12E, 12H). There are three other smaller lenses of Cu

enrichment. Two lenses are found along a trend which plunges into the WSW area of the deposit. The third lens is located about 200 feet below the main ore zone (Fig. 12E, 12H).

The Pd high grade zone has a minimum cut-off grade of 0.93 g/t. Unlike both the Cu and Au rich-areas, Pd grade large than 0.93 g/t does not centralize around any point (Fig. 12, 13, 14). This in mind, the Pd high grade zone (>.93g/t) does seem to show more extension at depth than it does at width. The lack of extent in the x and y direction is function of the dimensions of the zone polygons set while constructing the model. However the down whole extent of this greater than 0.93 g/t Pd zone does suggest that an extension with depth.

4.5 Bulk Rock geochemistry

Spider diagrams were constructed from the bulk rock geochemistry, and were normalized to a barren diorite from the Afton mine (Fig. 7, 8). Samples were grouped into different sections: those with the same alteration mineral, classified from IR-NIR spectroscopy (Fig. 7), and those with the same alteration assemblage (Fig. 8). The overall trends for all groups are similar, differences arrive due to the presence of multiple alteration assemblages and minerals within a given rock.

4.6 Laser ablation-induced coupled plasma mass spectroscopy (LA-ICPMS) of hematite in ore samples

Trace amounts of V, Cr, Co, Ni, Pd, Sn, and Au were found within the structure of hematite (Fig. 9). The presence of Pd within the structure of hematite indicates that Pd and hematite mineralization were a result of the same event, and thus the same mineralizing

fluids. Fluid inclusions within hematite will therefore be representative of the fluid responsible for the precipitation of Pd.

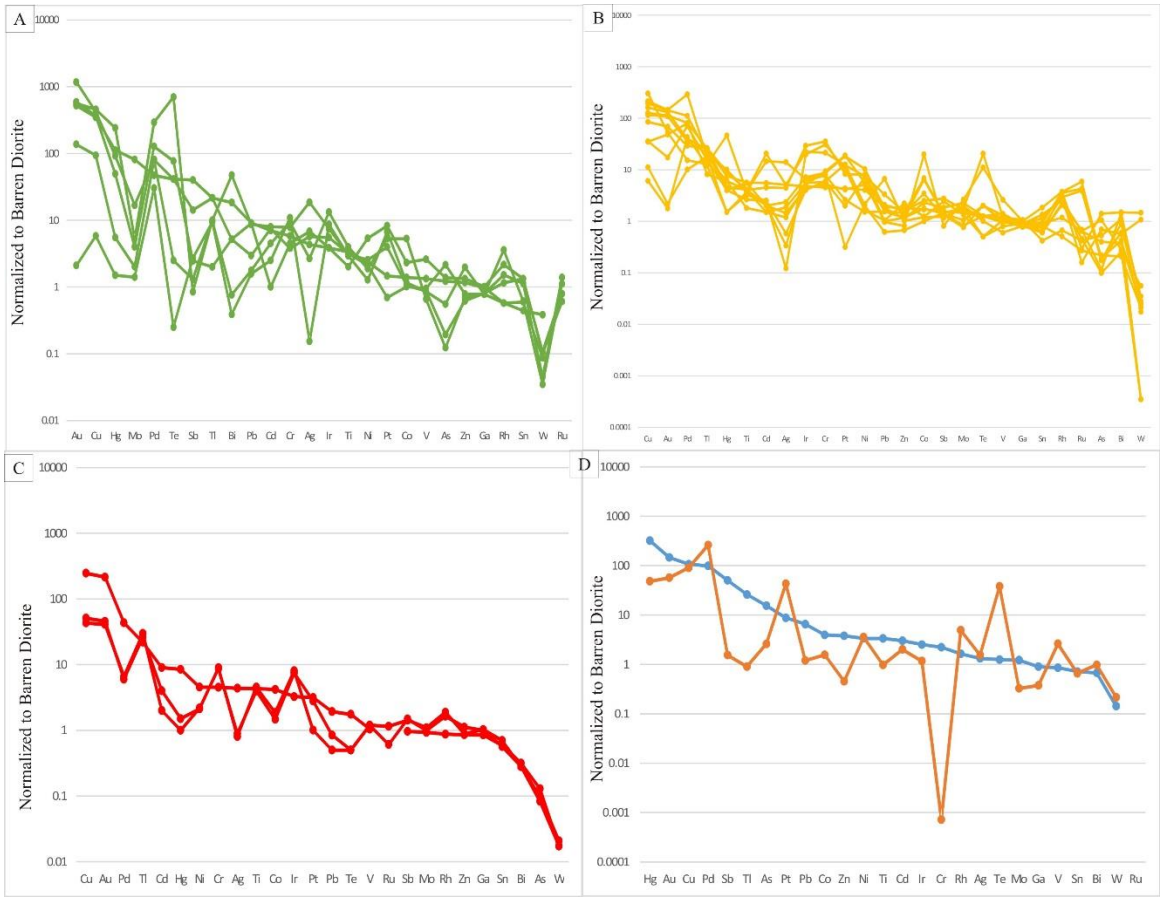

Figure 7. Spider Diagrams for different alteration assemblages, normalized to a barren diorite. (A) Propyllitic alteration. (B) Phyllic alteration. (C) Potassic alteration. (D) Argillic alteration. Featureless line is not a sample (related to formatting)

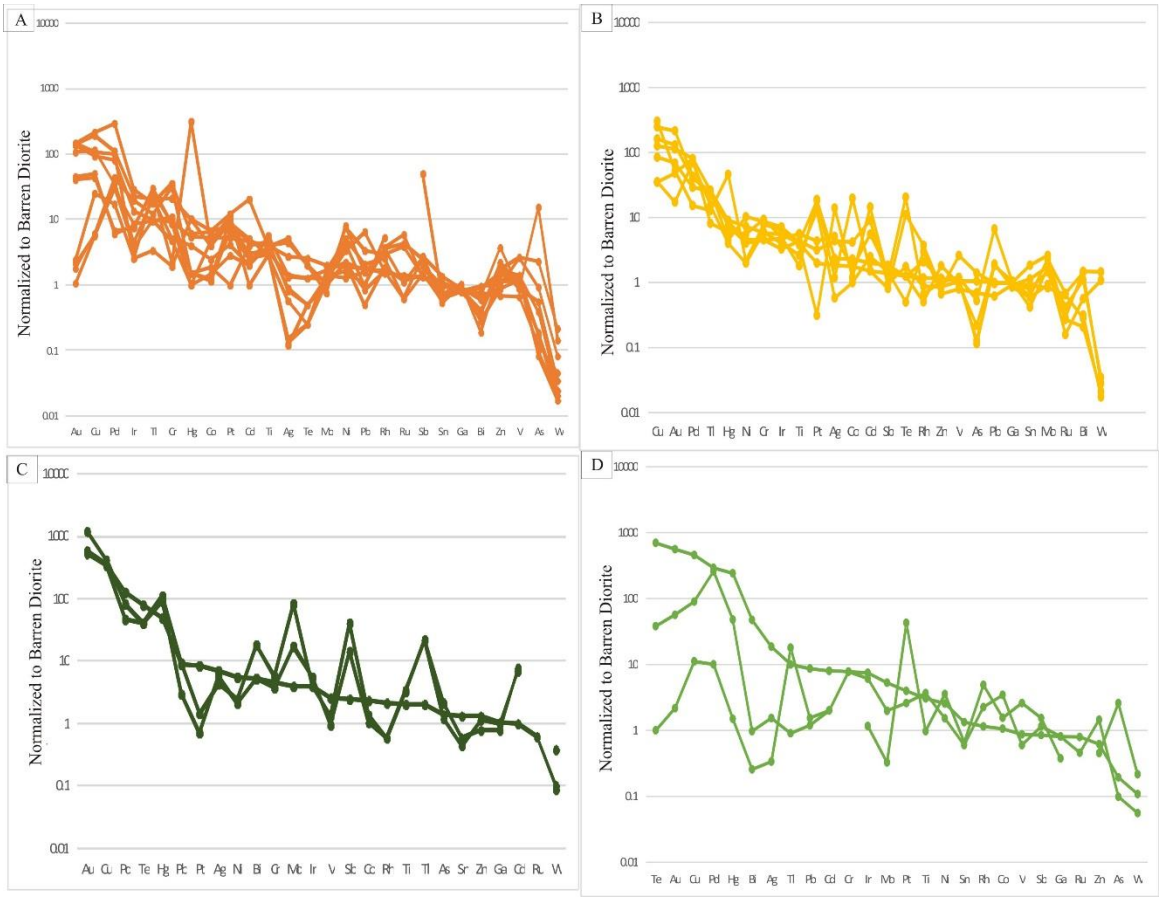

Figure 8. Spider Diagrams for different alteration minerals, normalized to a barren diorite. (A) High Al-dioctahedral mica. (B) Low Al-dioctahedral mica. (C) Mg-chlorite. (D) FeMg-chlorite. Featureless line is not a sample (related to formatting)

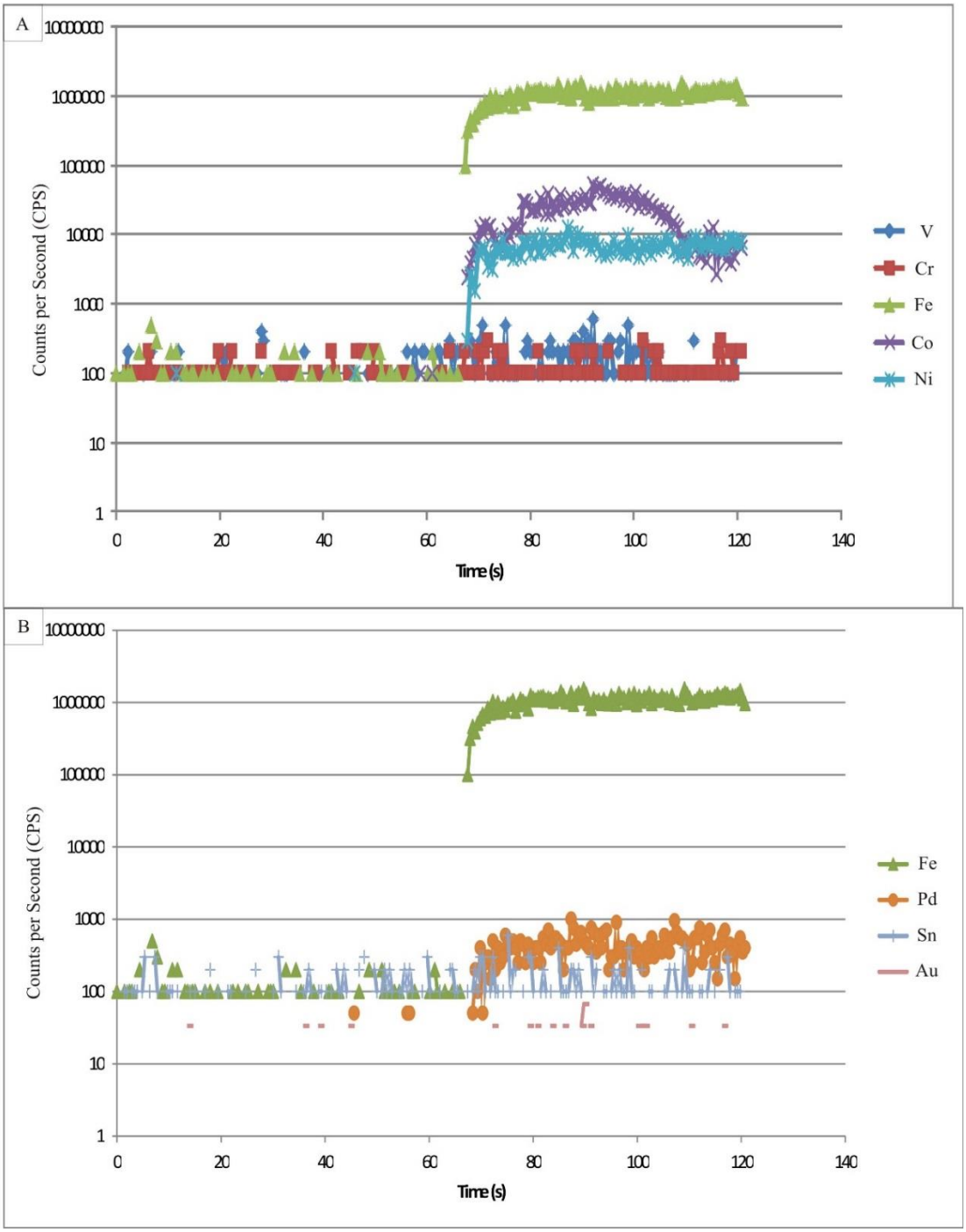

Figure 9. Transient signal from LA-ICPMS for hematite. (A) Fe is plotted with V, Cr, Co, and Ni. (B) Fe is plotted with Pd, Sn, Au. Palladium is present within the structure of hematite, indicating that Pd and hematite mineralization are related to the same event.

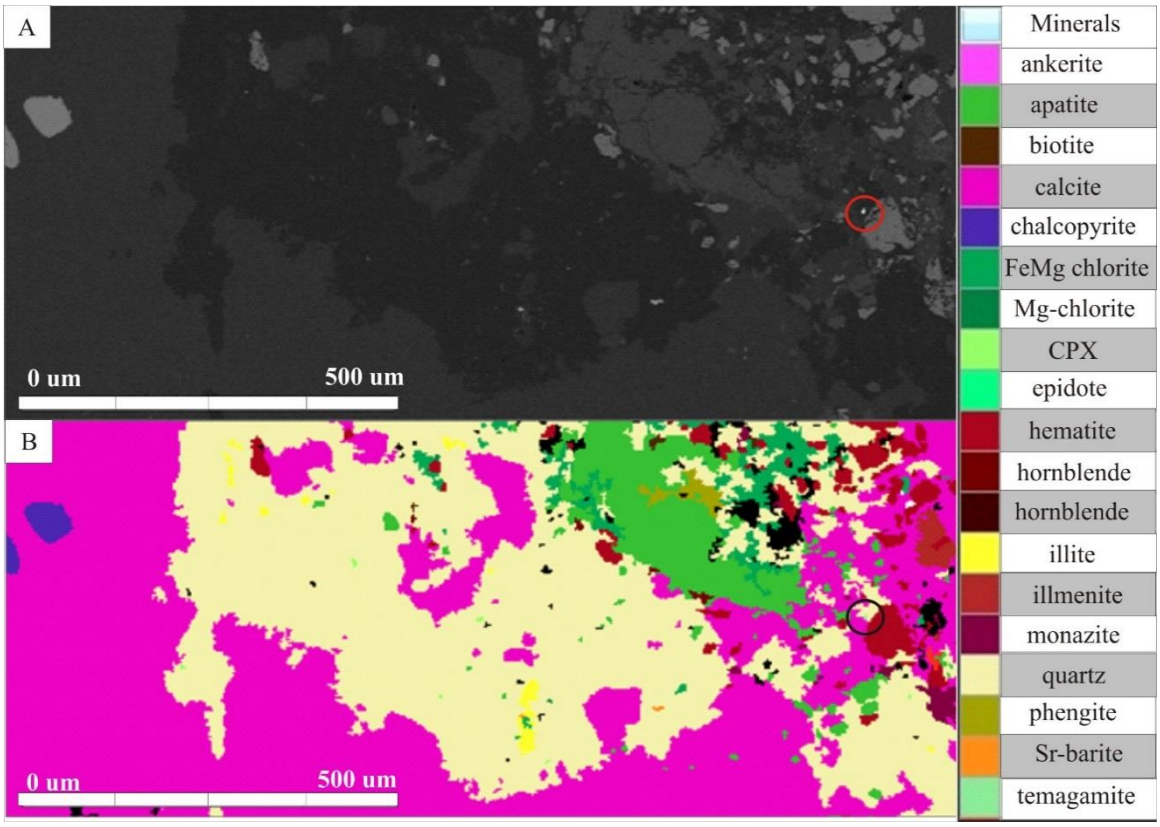

Figure 10. MLA image of UA50 241 created via SEM-MLA: (A) Backscatter image created via SEM-MLA. (B) Colour image created from backscatter image with the use of MLA software. Quartz-carbonate vein hosting hematite in close proximity to temagamite (circled white dot, in middle right side).

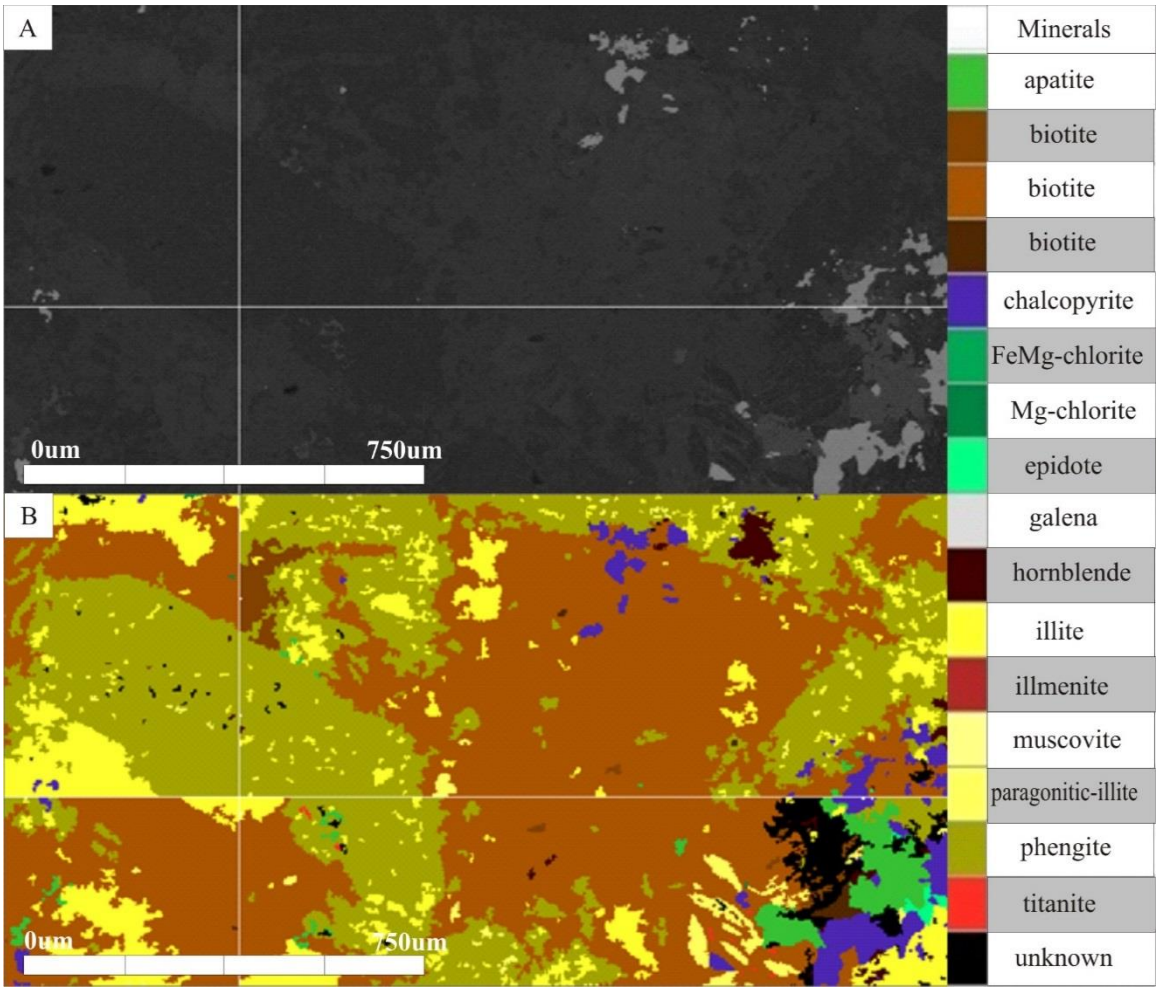

Figure 11. MLA image of UA50 245.4 created via SEM-MLA: (A) Backscatter image created via SEM-MLA. (B) Colour image created from backscatter image with the use of MLA software Secondary hydrothermal biotite dominates this section, with sericite-illite (phengite) replacing feldspar porphyroclasts. This replacement texture between phengite and presumably primary K-feldspar is common throughout the sample.

Table 2. MLA table depicting % of temagamite and mertieite-II grains hosted within a host mineral

Sample	# of grains	Target Mineral	Host Mineral	Binary Particle (%)	Ternary Particle (%)
UA44 348	3	mertieite-II	chalcopyrite		35.76
			phengite		21.79
			quartz		21.25
			illite		15.84
			biotite		3.41
			cpx		1.96
UA50 241	12	temagamite	apatite		34.94
			quartz	1.54	18.62
			FeMg chlorite		12.70
			calcite		8.52
			hematite	7.31	6.64
			monazite		5.20
			unknown		3.08
			chalcopyrite		1.46
UA50 245	1	temagamite	*Mg chlorite*		92.87
			chalcopyrite		7.13
	2	mertieite-II	*Mg chlorite*		55.72
			illite		19.23
			chalcopyrite		14.61
			phengite		6.35
			epidote		4.10

Binary particle % relates to situations in which the Pd bearing phase is hosted primarily within one host phase, where ternary particle % is a percent relates to situations in which the palladium bearing phases is in contact with multiple mineral phases. The binary and ternary particle % sum to 100 for each sample.

Table 3. MLA table depicting the modal mineralogy for each sample analyzed.

Sample	Mineral	Area%	Area (micron)	Grain Count	Particle Count
UA 44 348	phengite	25.13	4524827	3407	10460
	chalcopyrite	24.59	4273260	5259	14040
	illite	19.45	3502798	3300	14849
	quartz	6.23	1121535	998	1748
	Mg chlorite	5.63	1014515	1416	2730
	cpx	2.69	483658	1326	3119
	biotite	2.15	387075	878	1491
	hornblende	2.09	376124	1502	5097
	hornblende	1.82	327681	779	1650
	amphibole	1.54	277973	1041	2188
	biotite	1.47	265178	1347	3040
	FeMg chlorite	1.24	223117	401	599
	biotite	0.85	153505	649	1030
	pyrite	0.70	126239	135	182
	white mica	0.58	105051	548	984
	paragonitic-illite	0.49	88977	453	821
	white mica	0.48	86510	698	1320
	apatite	0.34	61091	200	255
	calcite	0.31	56591	223	335
	epidote	0.29	51940	150	226
	titanite	0.13	23629	377	605
	galena	0.09	16400	777	1310
	muscovite	0.04	7923	32	42
	bornite	0.03	4680	75	93
	ilmenite	0.02	3392	81	102
	hematite	0.01	1488	13	13
	unknown K phase	0.01	1252	19	19
	barite	0.00	859	39	41
	monazite	0.00	757	23	29

Sample	Mineral	Area%	Area (micron)	Grain Count	Particle Count
UA44 348	ankerite	0.00	425	7	7
	naumannite	0.00	208	9	11
	Sr-barite	0.00	185	7	8
	tantite	0.00	93	15	15
	clinochlore	0.00	83	3	4
	unkown Th phase	0.00	38	2	2
	bismuth	0.00	20	1	1
	electrum	0.00	16	2	2
	mertieite-II	0.00	14	3	3
	kurilite	0.00	13	1	1
UA50 241	quartz	27.60	4032086	2623	4973
	calcite	17.47	2551678	1672	3239
	apatite	16.22	2369753	2113	8130
	chalcopyrite	15.08	2202446	945	3041
	hematite	6.77	989558	1370	2853
	FeMg chlorite	3.91	570480	972	1770
	Sr-barite	2.01	294200	371	494
	titanite	0.48	164942	248	832
	bornite	1.13	164740	476	2333
	monazite	0.93	135167	806	1570
	hornblende	0.37	53993	538	870
	epidote	0.29	41760	172	224
	hornblende	0.25	36317	228	299
	amphibole	0.20	28649	251	325
	ankerite	0.18	25764	229	389
	pyrite	0.17	25002	23	50
	ilmenite	0.11	15554	82	157
	cpx	0.10	15185	262	516
	illite	0.05	7913	29	47
	electrum	0.04	6498	169	185
	biotite	0.03	5073	33	34
	Mg chlorite	0.02	2332	33	39
	white mica	0.01	1524	66	99
	hematite	0.00	1392	16	17
	white mica	0.01	843	6	6
	tantite	0.00	631	9	9
	biotite	0.00	588	9	10
	paragonitic-illite	0.00	519	3	3
	titanite	0.00	495	10	11
	phengite	0.00	320	7	7
	temagamite	0.00	295	12	12

Sample	Mineral	Area%	Area (micron)	Grain Count	Particle Count
UA50 241	galena	0.00	261	7	8
	chalcocite	0.00	123	8	8
	barite	0.00	77	6	6
	unknownTh phase	0.00	23	2	2
	bismuth	0.00	5	1	1
UA 50 245	illite	30.81	10558644	2328	12353
	chalcopyrite	29.98	10273314	2705	11670
	phengite	13.98	4790222	1868	8030
	paragonitic-illite	3.93	1348210	973	3278
	epidote	3.91	1338667	411	1836
	Mg chlorite	3.87	1326060	530	1272
	biotite	1.99	683152	190	505
	biotite	1.92	658693	656	1968
	biotite	1.72	588418	436	1680
	hornblende	1.50	514075	503	2264
	FeMg chlorite	0.94	323135	227	385
	calcite	0.77	264743	182	505
	amphibole	0.65	222159	308	761
	white mica	0.57	195379	469	1685
	pyrite	0.46	159128	25	88
	apatite	0.31	105667	117	238
	white mica	0.29	98169	430	1148
	quartz	0.27	91653	121	250
	ilmenite	0.10	34791	170	632
	muscovite	0.07	22817	20	24
	galena	0.05	16157	454	904
	cpx	0.04	14722	24	48
	bornite	0.03	11282	202	249
	barite	0.02	7551	94	104
	hornblende	0.01	3635	28	48
	naumannite	0.01	2653	21	23
	K-rich clay	0.01	1716	13	14
	Sr-barite	0.00	1434	28	30
	clinochlore	0.00	848	16	17
	unknownTh phase	0.00	427	7	7
	monazite	0.00	304	19	20
	electrum	0.00	294	8	9
	ankerite	0.00	68	3	3
	bismuth	0.00	67	1	1
	tantite	0.00	49	9	9
Sample	Mineral	Area%	Area (micron)	Grain Count	Particle Count

	cuprite	0.00	34	1	1
	Ag-Au-Cu-Zn	0.00	28	2	2
	mertieite-II	0.00	11	2	2
	sperrylite	0.00	9	1	1
UA50 245	temagamite	0.00	6	1	1

Particle count refers to the number of pixels/particles of each mineral was counted, where grain count is based on the number of actual mineral grains present in the sample, determined by the MLA software using the interaction of all particles adjacent to one another. The area represents the total area, in % and microns of the slide each mineral type occupied.

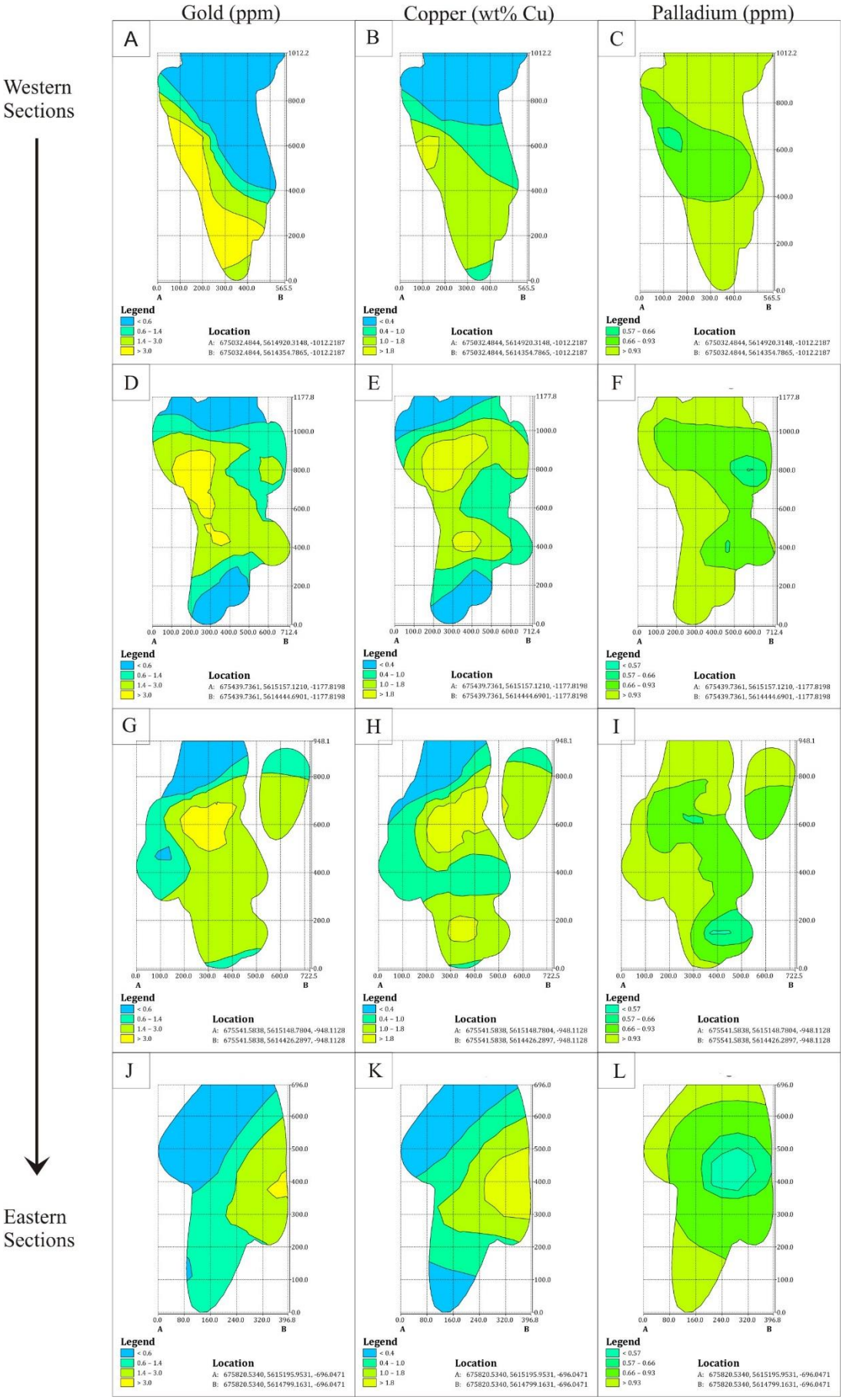
Gold (ppm)
Copper (wt% Cu)
Palladium (ppm)
Western Sections
Eastern Sections
A
B
C
D
E
F
G
H
I
J
K
L
Legend
Location

Figure 12. Westerly facing cross sections of Au in g/t (A,D,G,J), Cu in wt% Cu (B,E,H,K) and Pd in g/t (C,F,I,L), on previous page: Moving downward these cross sections represent the most western portion of the deposit (A,B,C), than the center of the model (D,E,F), than the area with the highest concentration of drill holes (G,H,I), followed finally by the eastern-most portion of the model (J,K,L). Pd high grade zones tend to show an inverse relationship with the high grade Cu, and to a lesser extend Au grades. Very clearly in Fig. 9L, it can be seen there is an outward zoning pattern exhibited by Pd grades.

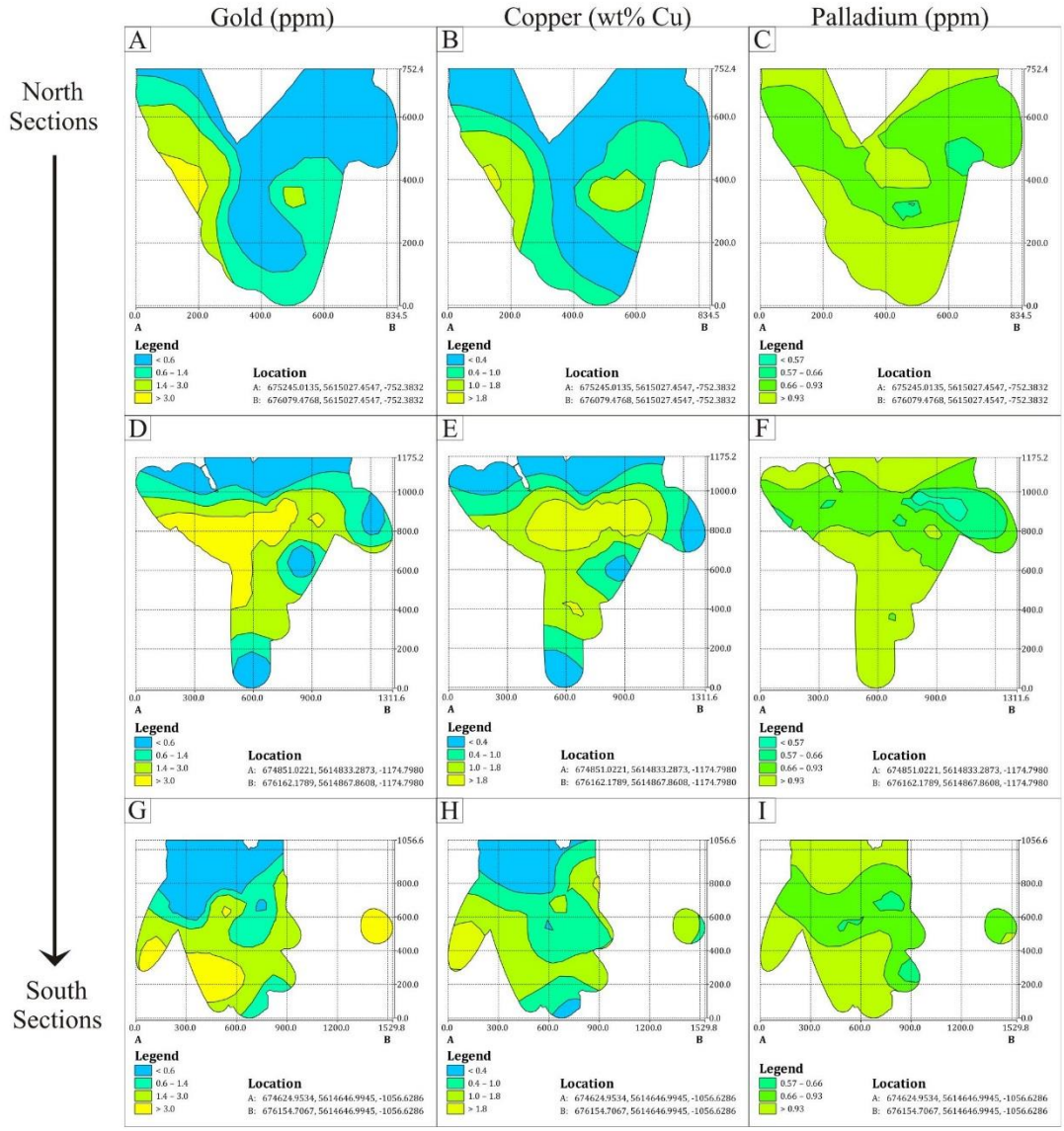

Figure 13. Northward facing long sections displaying Au grades in g/t (A,D,G), Cu grades in wt% Cu (B,E,H) and Pd grades in g/t (C,F,I): Sections A,B and C represent the N-most sections, with D,E and F representing the middle sections and G,H and I representing the southernmost sections. There is a nice representation of the southwesterly plunging Au structure in Figures D and G.

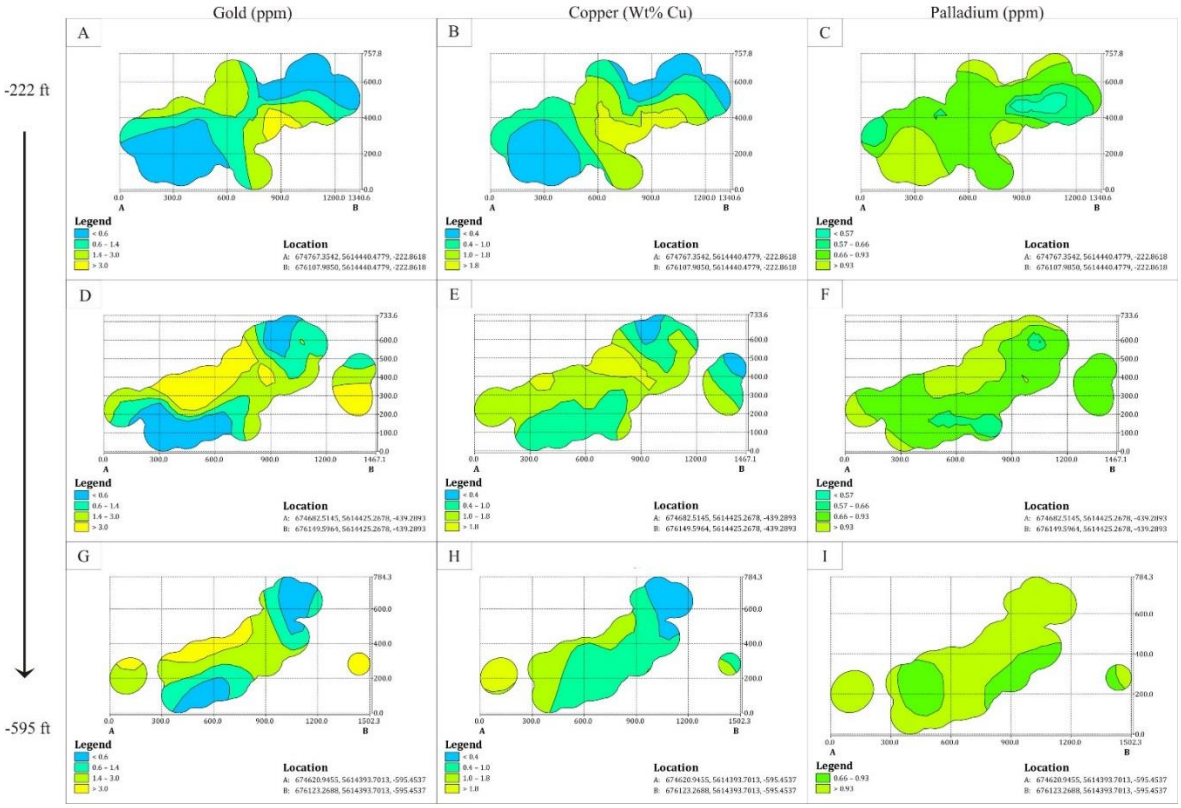

Figure 14. Downward facing plane sections displaying Au grades in g/t (A,D,G), Cu grades in wt% Cu (B,E,H) and Pd grades in g/t (C,F,I): Sections A,B and C represent the top most sections, with D,E and F representing the middle sections and G,H and I representing the bottom most sections

5.0 Discussion

5.1 Comparison to other systems

There are two rather similar alkaline porphyry system upon which Afton can be compared too. The first being Mount Milligan in British Columbia, and the second being Elatsite in Bulgaria. Mount Milligan is an alkaline porphyry deposit as is Afton, which contain significant PGE, specifically Pd mineralization. Unlike Milligan, the Afton ore zone contains only minimal pyrite, the majority of the sulfide mineralization is found in the form of chalcopyrite and bornite. Chalcopyrite, like pyrite in Milligan is found within and spatially associated with late stage quartz carbonate veins (LeFort et. al 2011) .The majority of Pd minerals at Afton are found associated with chalcopyrite and quartz with a minor amount located disseminated within the matrix. Gold at Afton is in the form of electrum and is hosted primarily as a disseminated phases within the matrix. Both electrum and Pd phases do not tend to be spatially associated with one another, thus unlike Milligan (Lefort et.al 2011) there appears to be separate events responsible for both Pd and Au mineralization. Palladium mineralization does however, although not strictly associated with Au, show a striking similarity to that at Mount Milligan. Like Mount Milligan, Pd is primarily hosted within telluride and arsenide/antimonide phases; temagamite and mertieite-II respectively. Associated with late quartz-carbonate fracture filling, these minerals do show similarities to those present at Mt Milligan.

The Elatsite deposit is hosted within a "granodiorite- monzodiorite" porphyry stock (Augé, et.al 2005), similar to that of Afton. This alkaline porphyry deposit has Pd present as the most important PGE. Similarly to Afton, Pd is hosted dominantly within tellurides at Elatsite (Augé, et al. 2005). Palladium at Afton is found within both tellurides and

antimonides, however the more prominent mineral phase is temagamite. The most widespread alteration assemblage at Elatsite is that of the phyllic zone (Petrunov & Dragov 1993). The majority of PGM are related to potassic alteration, characterized by hydrothermal biotite (Augé, et al. 2005). This observation can also be made at Afton with regards to selectively pervasive, fracture controlled hydrothermal biotite, which displays spatial association with PGM hosting quartz carbonate and chalcopyrite.

5.2 Spatial distribution of platinum group elements in relation to Au and Cu

Gold grades exceding 3.0 ppm and Cu grade larger than 1.9 wt% Cu have a strong positive correlation with one another (Table 12, Fig. 12-14). Both appear to have a main zone centred on the same location, and display a decrease in grade zoning outward from an approximately spherical domain (Fig. 12-14). Gold tends to show more lateral extent along the main structure which strikes approximately northeast (Fig. 12A, 12D, 12G, 12J), where the highest grade Cu zone (above 1.9 ppm) tends to its semi spherical shape (Fig. 12-14). When compared to the higher grades of Pd, characterized as anything above 0.93 ppm, there appears to be an inverse relationship. High grade Pd values tend to form a shell around the major Cu-rich zones (Fig. 12-14). They even appear, in some cases to inversely mirror the shape of the Cu-rich zones. The zones with the lowest grades in Pd appear within the highest grade zones of Cu, thus giving the image of a decreasing inward pattern (Fig. 12L). As Au has a positive correlation with Cu, Pd appears to show the same tendency to inversely shell around high Au grades. However, along the strike of the main structure there are many places in which high Au and Pd grades show a positive correlation (Fig. 12D, 12F; 13D, 13F; 14A, 14C). Thus, from the 3D model produced, it appears that there is a primary inverse zoning pattern between Cu and Pd, and a secondary positive correlation

between Au and Pd high grade zones along the main structure running through the center of the deposit, dipping to the south east (Dolbear, 2005). The highest grade Pd values are found (i) on the outermost reaches of the Cu porphyry system, and (ii) along the main structure with Au.

5.3 Relationship of platinum group elements and Au to alteration

Gold and Pd grades show varying correlation to one another (Table 1). Gold grades above 0.9 ppm can show a positive correlation with the presence of Mg-chlorite in the sample (Table 1). There are some cases where this is not true. Palladium grades exceeding 0.8 ppm can be found in the presence of a variety of hydrous silicates, but consistently, phengitic or paragonite dioctahedral micas and FeMg to Mg-chlorite are present. The presence of Mg-chlorite does not indicate an increase in Pd grade; this can only be said for Au in some cases. High Pd grade does not show an association with any specific alteration. In some cases high Pd grades exist in the presence of paragonitic and phengitic end member dioctahedral mica, and in other cases there is no correlation. Therefore, Pd can only be said to have precipitated in an environment in which paragonitic or phengitic dioctahedral micas could also be precipitate (see below).

5.4 Paragenesis

As both hydrothermal biotite (phlogopite) and phengitic or paragonitic illite are texturally related to one another in some samples, the mineral reaction below may be used to describe their formation (Formula. 1).

Formula: 1

$$(\mathrm{Mg,Fe})_3(\mathrm{Si,Al})_4\mathrm{O}_{10}(\mathrm{OH})_2\ (\mathrm{chlorite}) + 2\mathrm{KAlSi}_3\mathrm{O}_8\ (\mathrm{K-feldspar}) \rightarrow$$

$$K(Al, Mg)_2(OH)_2(Si, Al)_4O_{10}\ (\text{phengite}) +$$

$$K(Mg, Fe)_3AlSi_3O_{10}(OH, F)_2(\text{biotite}) + SiO_2 + H_2O(v)$$

Since the formation of phengitic or paragonitic illite may be associated with the precipitation of Pd, the expression above must characterize the conditions of Pd precipitation. With the dehydration of chlorite by heating and reaction with K-feldspar, the minerals phengite and biotite stabilize. For example, the presence of primary propylitic and potassic alteration or primary igneous K-feldspar, can be, if reheated by fluids produced from the degassing of the local Mg-basalt, converted to phengite and biotite. The degassing of this Mg-basalt can possibly provide the required Pd to mineralize this section of the deposit. The coprecipitation of phengite and biotite can be confirmed on a local scale along Pd bearing fractures, by the presence of equilibrium textures between biotite and phengite. Presence of local equilibrium between these two minerals was noted via petrography. Their presence in relation to Pd minerals was found through SEM-MLA. In addition to this, biotite commonly displays reaction and replacement textures with chlorite. Potassium feldspar appears to be replaced by phengite dioctahedral end member throughout the slides (Fig 2, 11). Therefore based on petrography, there is evidence to suggest this reaction may have played a part in the formation of alteration styles found in these samples, and may thus be related to Pd mineralization.

The mineral reaction above can be described in the system HCl-H_2O-(Al_2O_3)-K_2O-SiO_2. in which the stable mineral assemblage is controlled by Mg^{+2}/H^+ and K^+/H^+ ratios in the associated fluid phase, in addition to T and P (Bowers, et.al 1984). Importantly, the conditions at which phengite (muscovite) and biotite (phlogopite) can coexist equilibrium

is greatly restricted when talc is not a saturated phase to above 400ºC and 0.5 kbar (Fig. 12).

It is also important to note that the biotite is Cl-rich where it occurs with Pd minerals. The Cl content in these biotites is quite high compared to literature values of normal granites (Boomeri, et. al 2006). As the Cl-content in biotites is strongly controlled by the fluid composition rather than temperature and pressure, it is evident that the fluid responsible for the precipitation/crystallization of biotite and thus phengitic mica and Pd must have been Cl-rich. Literature suggests that biotite with higher concentrations of Fe partitions Cl over F into its structure. Chlorite has a higher partition coefficient for Mg than for Fe. In the presence of Mg- and Cl-rich fluid, chlorite would accept Mg cations over Fe cations, locally enriching the fluid in Fe. If biotite precipitates from a Fe rich solution, biotite would be relatively Fe rich. As Fe rich biotites tend to partition Cl over F, the Fe-rich biotite would become relatively enriched in Cl. The release of Cl^- anions from a solution would increase the pH of the fluid. This pH change could lead to the precipitation of Pd and Pt. As a result of these movements of Cl and Fe, the resultant sample would be left with Mg-chlorite and Fe/Cl-biotite. The concentration of Cl in biotite is however, more strongly affected by the Cl concentration in the fluid than it is by the concentration of Fe in biotite. Therefore, the precipitation of Cl-biotite can occur without first enriching biotite in Cl, if the fluid responsible for the mineral assemblage was rich in HCl (Boomeri, et. al 2006).

5.5 Hydrothermal Processes Associated with platinum group element deposition

Phengite, along with paragonite are dioctahedral micas and are hydrothermal alteration

products (Roberts and Hudson, 1983). These minerals are the main white micas in the samples analyzed from Afton. Aluminum content in dioctahedral micas can be estimated based off of N-IR spectroscopy. High Al dioctahedral micas tend to produce an absorption feature at 2.206um, where low aluminum dioctahedral micas produce a feature around 2.213 um (Tappert, et al. 2013). These absorption feature positions were located on the N-IR spectral data created for Afton and composed into Table 1. From this very small sample suite, there can be no association made with regards to Pd and specific dioctahedral micas, only that these two dioctahedral micas are the main and most important white micas in this ore sample suite.

Both phengite and paragonite are favored to precipitate in high pH conditions, however phengite precipitates in the presence of Mg rich fluids where the formation of paragonite requires very low Mg concentrations in solutions (Saccocia and Seyfried, 1994), such as Mg-depleted and alkali-enriched hydrothermal fluids (Edmond et al. 1995; Von Damm, 1995). As both of these minerals show a correlation with high Pd grade and the presence of paragonite requires fluid compositions that do not favor phengite, there may be two separate mechanisms for the precipitation of Pd, one in which a fluid has a high Mg concentration and the other which has a low Mg concentration. As Au, shows a positive relation toe the presence of Mg-chloride we can assume that the Mg rich fluid may be responsible for the Au precipitation, and this one event of Pd mineralization should be associated with that of Au. High Au grades (>3.0 g/t) concentrate along the large N-E trending structure, along with high Cu grade ellipses that occur at various locations in the 3D model. High Pd values on the other hand are inversely zoned around the Cu ellipses, but also occur along the same N-E trending Au structure.

As the primary structure is parallel to this N-E trending Au structure, it is evident that

this structure provided a pathway for the precipitating Au and association Pd. (Dolbear, 2004). It is also evident that Pd values larger than 0.93g/t exist in areas of greater than 3.0 g/t Au, the same zones present in close proximity to the major structure. Therefore, there seems to be two distinct environments in which large Pd grades are situated around: (i) those which are high in pH, high in Mg content and subsequently associated with the main fault striking N-E through the deposit, (ii) those which represent high pH zones associated with low Mg content, and high Na content.

It is also important to note that Pd becomes increasingly soluble under hydrothermal and low temperature conditions compared to other PGE (Augé, et al. 2005). In addition to this, the transport of palladium in chloride complexes at a high pH (<6), requires very strongly oxidizing conditions (Wood, 2003). As mentioned earlier, the presence of other metals in the fluid which favor the formation of complexes with chloride will reduce the solubility of Pd in solution (Economou-Eliopoulos, 2005). Therefore, the removal of such metals ions such as Cu^{+} would subsequently increase the relative availability of Cl^{-}, and the solubility of Pd in solution. Such an event could promote the dispersion of Pd into the far reaches of the deposit. Palladium would be required to remain in solution much longer to precipitate in the outer reaches of the deposit.

Picrite dykes can be found just above the hanging wall of the main structure, in the south west corner of the deposit (Dolbear, 2004). If these picrite dykes dip parallel to the main fault with depth, this rock unit could provide a solution with regards to one of the Pd occurrences. If this Au and Pd mineralization is a secondary event related to remobilization of Pd from the adjacent high Mg-basalts along this major structure, or

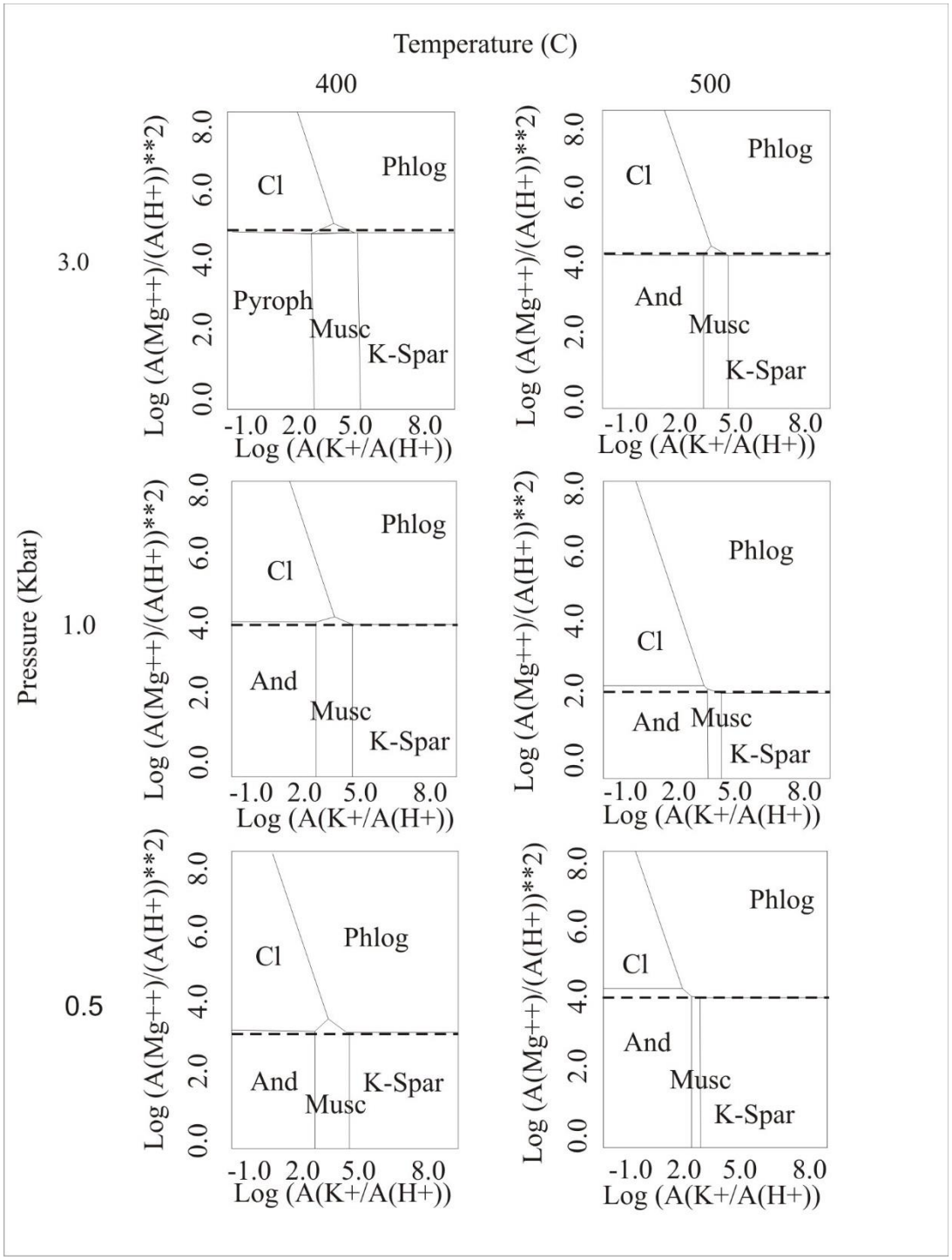

Figure 15. Phase relations in the system HCl-H_2O-Al_2O_3-K_2O-SiO_2 in equilibrium with quartz. Modified from Bowers et al (1984): The conditions under which phlogopite (phlog) and muscovite (musc) can coexist without the presence of talc; the talc saturation line is shown as a dotted line parallel to the x-axis.

remobilization of Pd from elsewhere in the deposit, than the dioctahedral mica forming in this near fault zone would be subject to high heat and pH from fluids flowing through this fault. In order for K-feldspar to be converted directly to phengite, there needs to be some iron and magnesium in the fluid (Tapper et al. 2013). If the surrounding syenites and diorites had previously been subject to potassic alteration, there would be little available Fe and Mg in the system, thus the addition of these elements from a fluid that has interacted with a picrite, for example, would prevent the formation of pure muscovite, which there is very little of in the samples, and favor the formation of a dioctahedral mica in which Mg and Fe are readily accepted into the structure (Formula. 2).

Formula: 2

$$3\mathrm{KAlSi_3O_8(K-feldspar)} + 2\mathrm{Mg^{2+}} + 2\mathrm{H^+} \rightarrow \mathrm{K(Al,Mg)_2(OH)_2(Si,Al)_4O_{10}(phengite)} + 2\mathrm{K^+} + 6\mathrm{SiO_2}$$

Subsequently, the conversion of K-feldspar to phengite requires acidic conditions. The production of phengite, can also form at the expense of muscovite, but instead requires a decrease in pH (Formula. 3).

Formula: 3

$$2\mathrm{K(Fe,Mg)_{0.5}Al_{1.5}Al_{0.5}Si_{3.5}O_{10}(OH)_2\ (phengite)} + 8\mathrm{H^+} + \mathrm{Al_2O_3} \rightarrow 2\mathrm{KAl_2AlSi_3O_{10}(OH)_2\ (muscovite)} + \mathrm{(Fe,Mg)^{2+}} + \mathrm{SiO_2} + 5\mathrm{H_2O}$$

As this near fault environment would be very hot and contain a high pH, phengitic end member micas would be favoured, as the addition Mg^{+2} and Fe^{+2} scoured from the picrite

would result in the formation of this mineral. Palladium solubility in chloride complexes can be transported by basic fluids only if the conditions are also strongly oxidizing (Gammons, 1996 & Wood, 2003).

If there are two separate mineralization events responsible for Pd, and if the secondary mineralization was sourced and remobilized from the high Mg-basalts, the question of the source for the outer shell Pd arises. Alkaline and potassic magmas can be created in suprasubduction zones, in which there is an availability of chalcophile elements, like Cu, Ni and PGE, to the magma in the mantle source and that involve oxidation of the mantle wedge from ferric iron in slab derived partial melts (Mungall et al. 2002). Therefore, PGE and Cu could have been present in the melt created by subduction of young lithosphere, which is characteristic of the subduction of the juan da fuca plate (McMillan, 1991), or slow, oblique or flat subduction (Augé, et.al 2005). Therefore, it is possible that the Pd present in the outer shell around the Cu rich zones are related to the magmatic properties of the porphyry deposit, where the other style of Pd mineralization is related to the remobilization of elements from local mafic rocks.

5.6 Preliminary evaluation of fluid inclusions and trace elements in ore associated hematite

There were no suitable inclusions found in any minerals, so hematite was investigated using IR. Hematite appears to be primary in most cases, however there are some cases of secondary hematite from magnetite. Hematite may provide the only opportunity to fully understand that ore precipitating fluids at Afton, and be used to answer some questions related to the possibility of late stage Pd mineralization. Many small inclusions were found within hematite using IR, however a few inclusions were large enough to present a possible opportunity for further studies (Fig 16). The largest inclusions were found within the largest

laths of hematite within groupings with smaller laths. The inclusions appear to be primary, as there are no immediate fractures in close proximity to the specific inclusion. Very few inclusion trails were found, and only in cases in which the inclusions were very small. However within one larger inclusion (Fig. 16H, 16I), there are few smaller inclusions on either side of it, which trace parallel to the edge of the crystal wall, perhaps, representing primary inclusion.

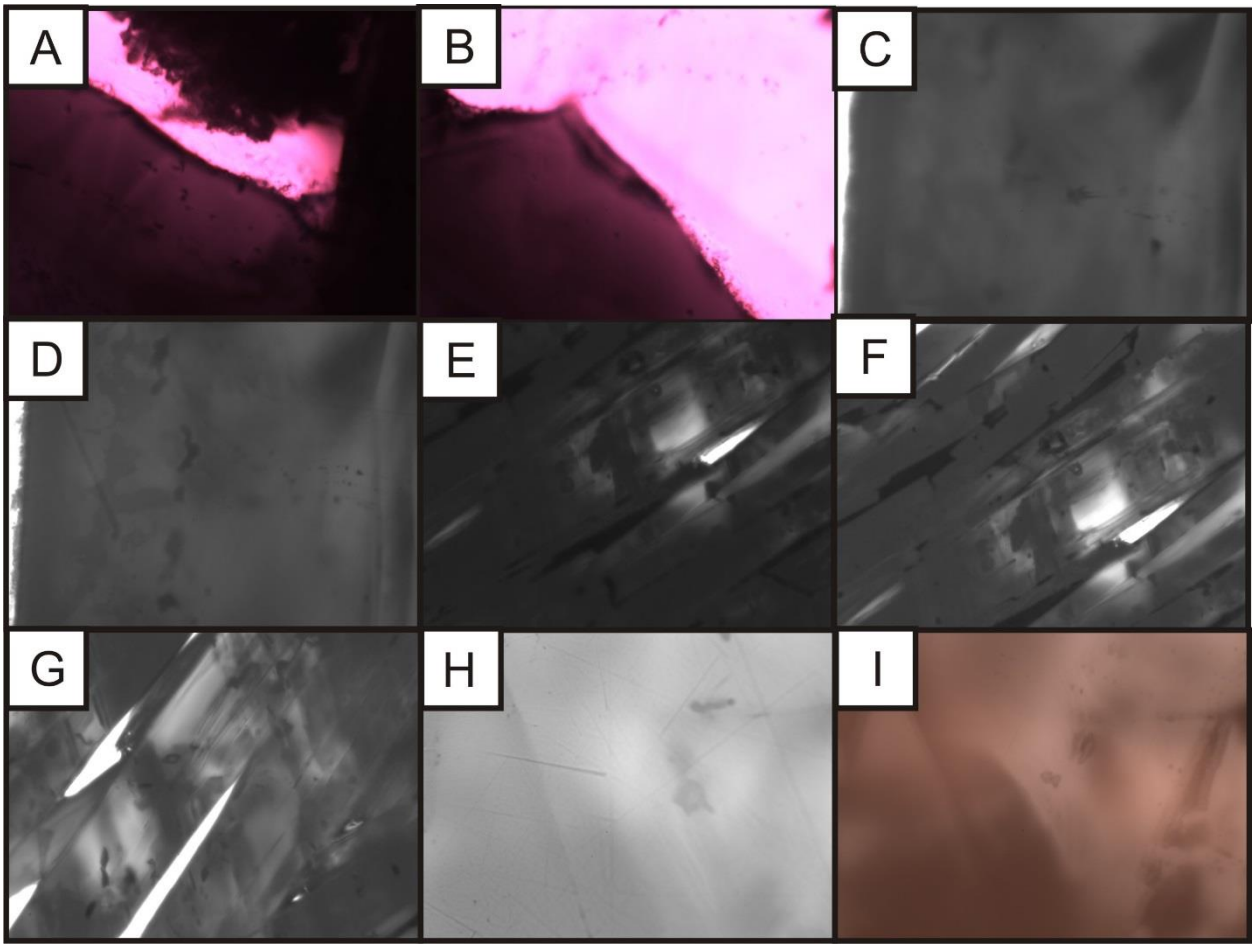

Figure 16. Fluid inclusions hosted within hematite: Hematite is spatially related to the palladium bearing phases and PGM bearing phases in the ore zone. Width of field is 320um

6.0 Conclusion

A mineralogical, NIR-IR spectroscopic, chemical, and spatial analyses of Pd- and Au-rich samples from the Afton porphyry system provide six conclusions:

(i) The major alteration minerals identified in the sample suite were chlorite (Mg to Fe-Mg), low-Al dioctahedral micas (phengite, phengitic illite, paragonitic illite), ankerite and epidote. The precipitation of the dioctahedral micas and Mg-chlorite occurs at high pH conditions; therefore we can conclude that the pH of the ore fluids would have to have been high at the time of Pd mineralization. The lack of high-Al dioctahedral micas (muscovite-illite-sericite), which are favored by acidic conditions, support this conclusion. Fluids responsible for the alteration and mineralization in these samples were also variably Mg-rich due to presence of phengitic illite, Mg-chlorite and ankerite. However, the presence of paragonitic illite would require either a second low Mg, high alkali fluid source, or represents the alteration product from a Mg-depleted fluid that produced zoned alteration systematics at the deposit scale (an alkali-rich fluid that depositing Mg-rich phases nearest its source, and then went onto crystallize paragonitic illite). The presence of Pd-enriched hematite indicates that these fluids were also oxidizing at the time of Pd transport.

(ii) From analysis of the created 3D model, it is evident that *primary* metal enrichments show that all four Cu(±Au) rich lenses with a grade larger than 1.8 g/t display an outward zoning pattern of decreasing grade, whereas Pd-enriched zones tend to decrease inward from an outer rich shell of Pd, with an inversed

relationship to that of the Cu(±Au) lenses (Fig. 12L). A Pd-Au-rich zone with a minimum cut-off at 3.0 ppm forming the center of an envelope, decreasing in grade outward, which plunges towards the WSW area of the deposit, formed by a *secondary* hydrothermal event.

(iii) Mg-chlorite commonly displays a correlation with high Au grades in the sample suite, indicating that the fluids responsible for the development of some of the highest Au grades were Mg-rich. There is no clear association of Pd with any alteration assemblage, other than the alteration assemblages that make up the whole sample suite (Fe-Mg-chlorite, phengitic illite, paragonitic illite). Future work should focus on more thorough spatial evaluation of the alteration to determine if these minerals are only characteristic of the areas sampled that represent the Pd-rich intersections in drill core, or if they are pervasive throughout the deposit, regardless of Pd grade.

(iv) From equilibrium diagrams and the occurrence of reaction textures between K-feldspar and dioctahedral micas, chlorite and biotite, along with the lack of of talc, it can be concluded that the system must have been at a temperature at between 400 and 500^{o}C and 0.5-3.0 kbar, when these minerals precipitate and reacted with one another. Since these minerals have a textural relationship to Pd-bearing minerals in the sample suite, it can again be concluded that these conditions also represent those present during their precipitation.

(v) High-grade Pd zones (>.93 g/t Pd) show a positive correlation with high grade Au zones (>3.0 g/t Au) and follow a trend similar to that of the main fault structure in the mine, plunging to the southwest. Adjacent to this structure, in the hanging wall on surface there is a high Mg basaltic (“picrite”) dyke. The

presence of secondary fluids flowing along this main fault could have remobilized Pd, Mg and alkalis from the basalt and buffered these fluids at higher pH. Alternately, degassing of a high pH, oxidizing fluid from the basalt could have carried Pd into the ore zone along with Mg, alkalis and possibly magmatic CO_2. The presence of Mg-rich chloride and paragonite and phengitic-end member dioctahedral micas (both of which favor basic conditions), associated with Au and Pd in this area would support this conclusion of secondary mineralization of Pd in this zone.

(vi) The main PGE minerals present in the ore suite analyzed by SEM-MLA are temagamite, and mertieite-II. Important texturally associated phases for these minerals include quartz, hematite, carbonates, chlorite and low-Al dioctahedral micas. Where chalcopyrite and apatite were identified as important host phases, these should not be considered to be genetically coeval hosts for the Pd carriers, since these minerals were brecciated by secondary mineralizing events and infilled by true (coeval) host phases for the Pd. The brecciation of the main Cu phases (chalcopyrite/bornite) and overprinting by Pd-bearing phases and associated *quartz-carbonate-hematite-chlorite-phengite/paragonite* demonstrates a secondary Pd-mineralizing event.

From these results one can produce some lose exploration requirements for Pd at the Afton porphyry system and may relate to other similar alkaline Cu, Au, Pd porphyry systems. As a suggestion for further studies, there are suitable fluid inclusions hosted within primary hematite related to the precipitation and mineralization in the ore zone, for analyses in which more light can be shed on the chemistry of the ore bearing fluids. In addition to

this, there is a need for an extensive IR-NIR investigation of all Pd bearing samples in the deposit to extend to comprehension of the presence of phengite to that of Pd.

7.0 References

Allen, R.L., Barret, T.J., Browne, P.R.L., Clemson, J.E., Dunne, K.P.E., Ettlinger, A.D., Gibson, H.L., Groat, L.A., Hannington, M.D., Hawke, M.M., Jowett, E.C., Lang, J.R., et. al, 2011, Atlas of Alteration: A field and petrographic guide to hydrothermal alteration minerals (Thombson, A.J.B & Thombpson J.F.H eds.): Geologic Association of Canada, Mineral deposits devision,1996.

Augé, T., Petrunov, R., Bailly., L., 2005, On the origin of the PGE mineralization in the Elastite porphyry Cu-Au deposit, Bulgaria: Comparison with the Baula-Nuasahi complex, India, andother alkaline PGE rich porphyries: The Canadian Mineralogist, v. 43, p. 1355-1372.

Boomeri, M., Mizuta, T., Ishiyama, D., Nakashima, K., 2006, Fluorine and chlorine in biotite from the Sarnwosar granitic rocks, northeastern Iran: Iranian Journal of Science and TechnologyTransaction A Science 30(A1): 111-125.

Bowers, T.S., Jackson, K.J., Helgeson, H.C., 1984, Equilibrium activity diagrams fo r coexisting minerals and aqueous solutions at pressures and temperatures to 5kb and 600 °C: Springer-Verlag, Berlin.

Dolbear, B., 2004, Mineral resource estimate for the afton copper/gold project, Kamloops, B.C.: Behre Dolbear & Company, Ltd. Vancouver, British Columbia.

Economou-Eliopoulos, M., 2005, Platinum group potential of porphyry deposits: Mineralogical Association of Canada Short Course Series Volume 35. In J.E. Mungall (Ed.), Exploration for deposits of Platinum-Group Elements, Oulu, Finland p. 203-246.

Edmond, J.M., Campbell, A.C., Palmer, M.R., German, C.R., Klinkhammer, G.P., Edmonds, H.N., Elderfield, H., Thompson, G., and Rona, P., 1995, Time-series studies of vent fluids from the TAG and MARK sites (1986, 1990): Mid-Atlantic Ridge: a new solution chemistry model and a mechanism for Cu/Zn zonation in massive sulfide ore bodies. In Parson, L.M., Walker, C.L., and Dixon, D.R. (Eds), Hydrothermal vents and processes. Geol. Soc. Spec. Publ. London, v. 87, p. 77-86

Eliopoulos, D.G., Economou-Eliopoulos, M., Strashimirov, S.T., Kovachev, V.,Zhelyaskova-Panayotova, M., 1995, Gold, platinum and palladium content in porphyry Cu deposits from Bulgaria: a study in progress: Geol. Soc. Greece v. 5, p. 712-71.

Gammons, C.H., 1996, Experimental investigations of the hydrothermal geochemistry of platinum and palladium. 5. Equilibria between platinum metal, Pt(II), and Pt(IV) chloride complexes at 25 to 300 degrees C: Geochim. Cosmochim. Acta v. 60, p. 1683-1694.

Guillong, M.M., Maier, D.L., Allan, M.M., Heinrich, C.A., and Yardley, B.W.D., 2008, Appendix A6: SILLS: a MATLAB based program for the reduction of laser ablation ICP-MS data of homogeneous materials and inclusions, *in* Sylvester P., ed., Laser Ablation ICP-MS in the Earth Sciences: Current Practices and Outstanding Issues: Mineralogical Association of Canada Short Course Series, v. 40, 6 p.

Günther, D., and Heinrich, C., 1999, Comparison of the ablation behaviour of 266 nm Nd: YAG and 193 nm ArF excimer lasers for LA-ICP-MS analysis. Journal of Analytical atomic Spectrometry, v. 14, p. 1369-1374.

Kiousis, G., Economou-Eliopoulos, M., Paspaliaris, J., Mitsis., J,. 2005, Gold, palladium and platinum recovery as by-product from the Skouries porphyry Ca-Au deposit at Chalkidiki area, N. Greece- preliminary results: Mao,J. & Bierlein, F.P (Eds), 8th SGA meeting, "mineral deposits research meeting the global challenge", Beijing. P. 991-994.

LeFort, D., Hanley, J., Guillong, M., 2011, Subepithermal Au-Pd mineralization associated with an alkali porphyry Cu-Au deposit, Mount Milligan, Quesnel Terrane, British Columbia, Canada: Economic Geology, v. 106. p. 781-808.

McMillan, W.J., 1991, Overview of the tectonic evolution and setting of mineral deposits in the Canadian Cordillera. In W.J Mcmillan, T. Hoy, D.G. Maclntyre, J.L. Nelson, G.T. Nixon, J.L. Hammack, A. Panteleyev, G.E. Ray & I.C.L Webster (Eds), Ore Deposits, Tectonics and Metallogeny in the Canadian Cordillera, Vancouver, British Columbia p. 5-24.

Mihalynuk, M., Logan, J., Ullrich, T., Friedman, R., 2006, Geology and mineralization of the Iron Mask Batholith: Geology survey of Canada.

Mortimer, N., 1987, The Nicola Group: Late Triassic and early Jurassic subduction related volcanism in British Columbia: Canadian Journal of Earth Sciences, v. 24, p. 251-2536

Mungall, J.E., 2002, Roasting the mantle: slab melting and the genesis of major Au and Au-rich Cu deposits: Geology v. 30, p. 915-918

Petrunov, R., Dragov, P., 1993, PGE and gold in the Elacite porphyry copper deposit, Bulgaria: In Current Research in Geology Applied to Ore Deposits (P. Fenoll Hach-Alí, J. Torres-Ruiz & F. Gervilla, eds.): Proc. Second Biennial SGE Meeting (Granada), p. 543-546.

Pettke, T., Halter, W. E., Webster, J. D., Aigner-Torres, M., and Heinrich, C.A., 2004, Accurate quantification of melt inclusion chemistry by LA-ICP-MS: a comparison with EMP and SIMS and advantages and possible limitations of these methods: Lithos, v. 78, p. 333-361.

Roberts, D.F., Hudson, G.R.T., 1983, The Olympic Dam copper-uranium-gold deposit, Roxby Downs, South Australia: Economic Geology, v. 78, p. 799-822.

Saccocia, P.J. and Seyfried, W., 1994, The solubility of chlorite solid solutions in 3.2 wt% NaCl fluids from 300-400 ^{0}C, 500 bars, Geochim. Cosmochim. Acta, V. 58, p. 567-585.

Tappert, M.C., Rivard, B., Giles D., Tappert, R., Mauger, A., 2013, the mineral chemistry, near-infrared, and mid-infrared reflectance spectroscopy of phengite from the Olympic Dam IOCG deposit, South Australia: Ore Geology Reviews, v. 53, p. 26-38.

Thompson, J.F.H., Lang, J.R., Stanley, C.R., 2001: Platinum group elements in alkaline porphyry deposits, British Columbia: Exploration and Mining in British Columbia, Mines Branch, Part B p. 57-64.

Wood, B.W., 2002, The aqueous geochemistry of the platinum-group elements with applications to ore deposits. In Geochemistry, mineralogy, metallurgy and beneficiation of PGE Geology. Cabri, L.J. (ed.): L Can. Inst. Mining Metall. Special Paper vol. 54, p. 211-249.

Von Damm, K.L., 1995, Controls on the chemistry and temporal variability of fluids. In Lupton, J., Mullineaux, L., Zierenberg, R. (Eds.), Physical Chemical, Biological and Geological Interactions within submarine hydrothermal sysytems. Am. Geophys. Union, Geophys. Monogr. V. 91, p. 85-114.